Recycling Process Development with Integrated Life Cycle Assessment – A Case Study on Oxygen Transport Membrane Material

Melanie Johanning, [a],[†] Marc Widenmeyer, [a]* Giamper Escobar Cano, [b] Vanessa Zeller, [c] Sebastian Klemenz, [d] Guoxing Chen, [d] Armin Feldhoff, [b] and Anke Weidenkaff [a],[d]

[a.] *Technical University of Darmstadt, Research Division of Materials & Resources, 64287 Darmstadt, Germany.*

[b.] *Leibniz University Hannover, Institute of Physical Chemistry and Electrochemistry, 30167 Hannover, Germany.*

[c.] *Technical University of Darmstadt, Research Division of Material Flow Management and Resource Economy, 64287 Darmstadt, Germany.*

[d.] *Fraunhofer Research Institution for Material Recycling and Resource Strategies IWKS, 63755 Alzenau, Germany.*

[†] *Present address: Ecole polytechnique fédérale de Lausanne EPFL, Laboratory for Molecular Engineering of Optoelectronic Nanomaterials LIMNO, 1015 Lausanne, Switzerland.*

Content

LCNC synthesis and recycling

The chemicals used for the primary synthesis and recycling of LCNC are listed in Table S1. All chemicals were used as purchased. The process flows for the Pechini-based primary synthesis and the developed recycling process are shown in Figure S1 and S2, respectively. The pre-calcination step was conducted using a Nabertherm L3/S17 (1.1 kW) furnace. For the calcination, a Nabertherm L3/12 (1.3 kW) or Nabertherm L5/12 (2.6 kW) furnace was used. Stainless steel grinding balls and jars were used for the ball milling of the pre-calcined precursors.

Table S1: Overview of utilized chemicals and suppliers.

| Chemical	Formula	Abbreviation	Supplier	Purity
Lanthanum (III) nitrate hexahydrate	$La(NO_3)_3 \cdot 6\ H_2O$	$La(NO_3)_3$	Alfa Aesar	99.9 %
Calcium (II) nitrate tetrahydrate	$Ca(NO_3)_2 \cdot 4\ H_2O$	$Ca(NO_3)_2$	Sigma Aldrich	99 %
Nickel (II) nitrate hexahydrate	$Ni(NO_3)_2 \cdot 6\ H_2O$	$Ni(NO_3)_2$	Alfa Aesar	98 %
Copper (II) nitrate hemipentahydrate	$Cu(NO_3)_2 \cdot 2.5\ H_2O$	$Cu(NO_3)_2$	Alfa Aesar	98–102 %
Citric acid monohydrate	$HOC(CO_2H)(CH_2 CO_2H)_2 \cdot H_2O$	CA	Carl Roth	> 99.5 %
Ethylenediaminete traacetic acid	$[CH_2N(CH_2CO_2H)_2]_2$	EDTA	Carl Roth	> 99 %
Ammonia solution (25 %)	$NH_3 + H_2O$	Ammonia solution	Carl Roth	Ultra-pure
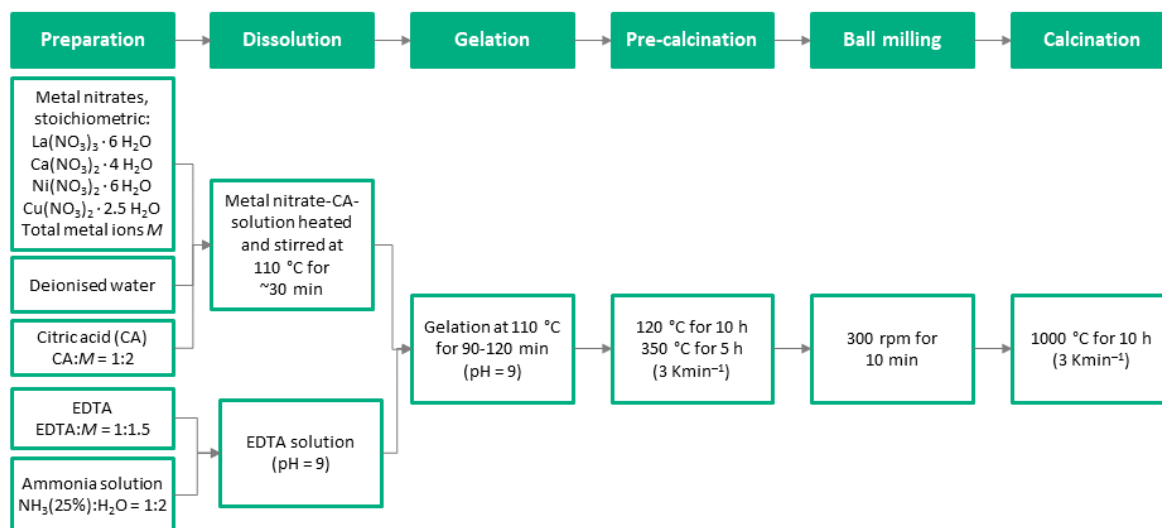
Figure S1: Process flow for the synthesis of LCNC from primary metal nitrates using a Pechini-based soft chemistry method.
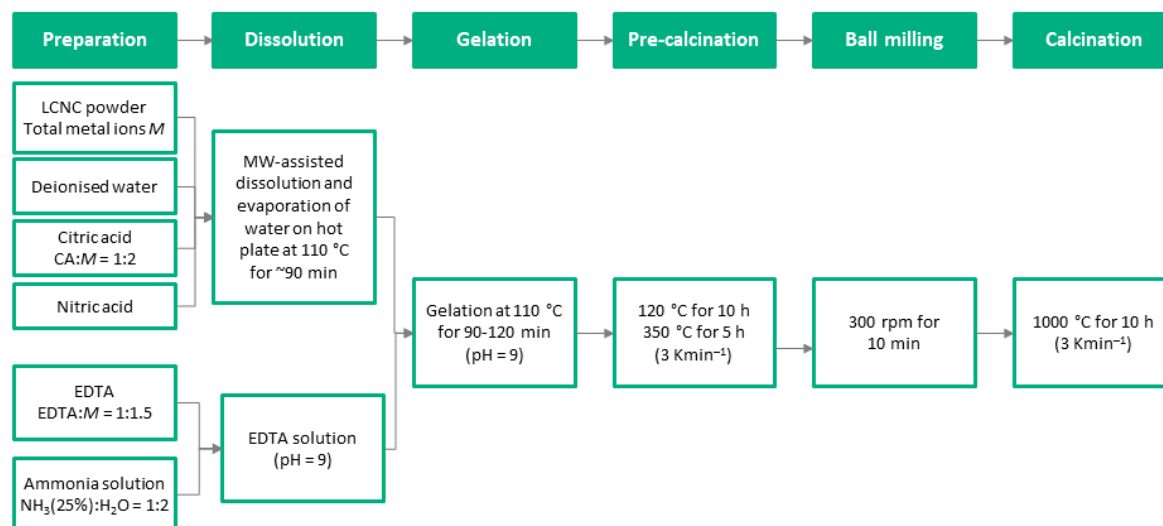
Figure S2: Process flow for the recycling of LCNC from primary LCNC powder by the developed method involving microwave-assisted dissolution and Pechini-based material reformation.

To produce a homogeneous LCNC precursor solution for recycling, the addition of nitric acid is crucial. Preliminary dissolution experiments of LCNC in an aqueous citric acid solution at 170 °C resulted in a turbid, greenish solution with white precipitates (see Figure S3). Energy-dispersive X-ray spectroscopy (EDXS) and powder X-ray diffraction (PXRD) identified the precipitate as lanthanum citrate (see Figure S4). The presence of lanthanum citrate is also supported by literature. Lanthanum citrate can be synthesised at conditions comparable to the chosen dissolution conditions [1,2]. The precipitates can be dissolved within several minutes by the addition of nitric acid and stirring at ~80 °C on a hot plate (see Figure S3). Therefore, nitric acid was added directly to the aqueous citric acid solution prior to the microwave-heated dissolution of LCNC. The minimum required amount of nitric acid was identified by a parameter study with a constant amount of water (200 mL restricted by the microwave autoclave) and molar ratios of citric acid CA to total metal ions M of 2:1 and 4:1. Dissolution at CA:M of 2:1 and 4:1 worked equally well. Therefore, the lower amount similar to that of the primary synthesis was chosen for recycling (2:1). Addition of 13 mL nitric acid was required for the chosen conditions. The dissolution temperature under addition of nitric acid is limited to 110 °C to prevent chemical decomposition. Other acids (e.g., hydrochloric acid) might also enable the formation of a homogeneous solution. However, nitric acid offers the advantage of easily removable anions, which is crucial for the Pechini-based processing.

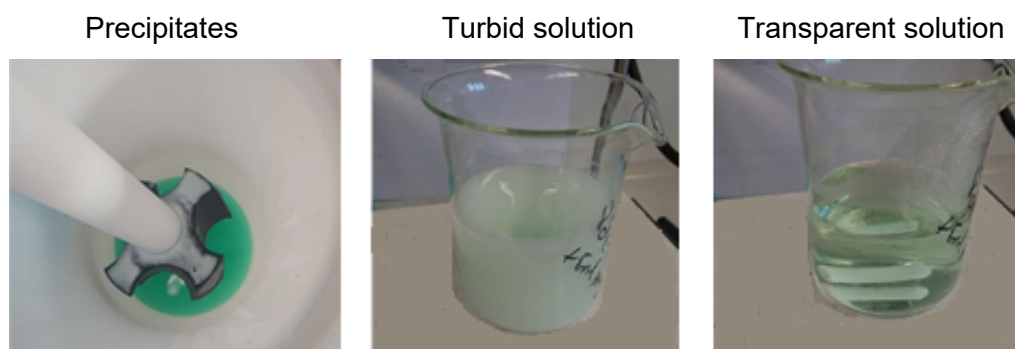| Precipitates	Turbid solution	Transparent solution

Figure S3: Turbid solution with white precipitates right after dissolution (left), turbid solution stirring at ~ 80 °C on the hot plate (middle), and transparent solution several minutes after addition of nitric acid (right).
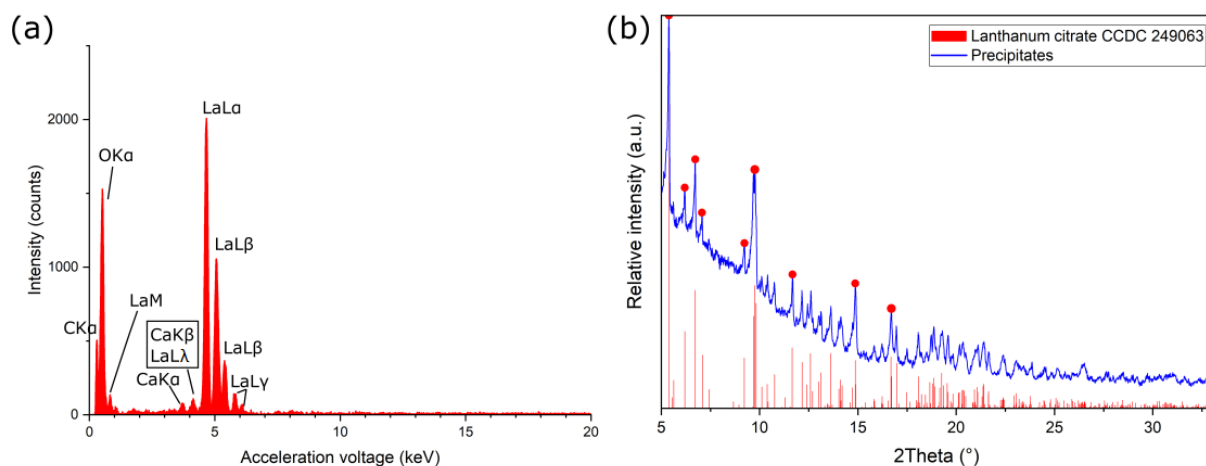
Figure S4: EDXS spectrum with assigned emission lines (a) and PXRD pattern (b) of the white precipitate. The measured XRD reflections with highest intensity were assigned to the main reflections of lanthanum citrate trihydrate [2].

Experimental characterisation

Additional experimental details regarding the experimental characterisation of the synthesised LCNC powders is provided in the following section.

For powder X-ray diffraction (PXRD), the measuring time was 150 s at each point with a step size of 0.015° in transmission mode with fixed 2Θ-ω-ratio. The main phase and potential impurity phases were identified using Match! software (version 3.12) [3] and the included Crystallography Open Database (COD, COD Inorg 14.06.2021) [4–10]. Afterwards, the phase composition and crystal structure of the products were assessed by Rietveld refinements using FullProf.2k (version: 7.00) [11] and pseudo-Voigt functions to describe the profile of the diffraction peaks.

The scanning electron microscope (SEM) (PHILIPS XL30) was equipped with an EDAX CDU Leap detector. An acceleration voltage of 10.0 kV and a spot size of 4.0 nm were used for imaging. Genesis Spectrum Software (version 5.2.1) [12] was used for elemental analysis by EDXS. The acceleration voltage was set to 30 kV and the spectrum at each point was acquired for around 15 min (stopped manually). No calibration by internal standards was conducted. Three different spots were measured for each sample and the average composition was calculated.

The thermal analysis of the reaction was conducted by TGA-DTA using Netzsch STA 409 and analysed by the thermal analysis software Netzsch Proteus (version 6.1) [13]. The measurements were conducted under a compressed air flow of 90 mL min^{-1}. Compressed air was purified by an Entegris Gatekeeper to remove CO_2, H_2O, and hydrocarbons.

The gas flow parameters for combined thermogravimetric (TG), mass spectroscopy (MS), and Fourier-transformed infrared spectrometry (FTIR) analysis were set as compressed synthetic air flow of 40 mL min^{-1} as reactive gas and nitrogen flow of 20 mL min^{-1} as protective gas.

Membrane discs were produced from primary and recycled LCNC powder. After manual grinding, green bodies in disc shape were formed by uniaxial (10 kN for ~5 min, P/O/Weber warm press, diameter 16 mm) and subsequent isostatic pressing (700 kN for 1.5 min, P/O/Weber KIP 100E) at ambient temperatures. Single step uniaxial pressing as conducted by Chen et al. [14] was not possible due to practical reasons. The discs were sintered at 1050 °C for 20 h in ambient atmosphere with a heating and cooling rate of 3 K min^{-1}. Sintered discs were subjected to phase analysis by XRD using similar parameters as for PXRD but in reflection mode.

The obtained sintered bodies were cut in two halves using a precision diamond wire saw (well 3500) to preadjust the thickness of the membranes. The membranes were grinded using sandpaper with the steps 600, 800, and 1000 to obtain the desired thickness of 0.65 mm and a defined surface. One membrane from recycled LCNC was selected for the permeation measurement. The second half and primary membranes were used to examine the density of the samples geometrically and by Archimedes principle after vacuuming of the samples. Water was used as a fluid.

The oxygen permeation flow of a membrane from recycled LCNC was determined under an air/CO_2 gradient at 900 °C for 24 h. Gold conducting paste (Chempur #902904) was utilised to fix the membrane on the alumina tube. The flow rate of synthetic air (20 vol.% O_2 and 80 vol%. N_2) was 150 mL min^{-1} on the feed side. The flow rate of CO_2 was 29 mL min^{-1} on the sweep side. An online-coupled Agilent 7890A gas chromatograph equipped with a Carboxen® 1000 column was employed to analyse the gas mixture. Neon with a flow of 1 mL min^{-1} was used as an internal standard to calculate the absolute flow rate. Further details of the experimental setup can be found elsewhere [15].

The morphology of the membrane surface and cross sections were compared for membranes from primary and recycled LCNC powder. The SEM was operated at the conditions described above. As preparation, the membrane was cut using the same diamond wire saw and sputtered with gold to avoid charging effects (30 mA for 45 s using Quorum Q300TD).

Crystal structure analysis – Rietveld refinements

Table S 2: Summarised Rietveld refinement results of primary and recycled LCNC.

	Primary LCNC	**Recycled LCNC**
Space group	*I4/mmm*	
a (Å)	3.82202(5)	3.82246(3)
c (Å)	12.7388(3)	12.7485(2)
V (Å³)	186.085(6)	186.270(2)
z(La/Ca)	0.3609(2)	0.3616(1)
z(O(1))	0.172(1)	0.177(1)
B_{iso}(La/Ca) (Å²)	0.55(5)	0.38(4)
B_{iso}(Ni/Cu) (Å²)	0.6(1)	0.37(9)
B_{iso}(O(1)) (Å²)	0.6(3)	0.3(2)
B_{iso}(O(2)) (Å²)	= B_{iso}(O(1))	= B_{iso}(O(1))
w(La) (-)	0.91(2)	0.91(2)
w(Ca) (-)	0.09(2)	0.09(2)
R_p (%)	12.0	10.7
R_{wp} (%)	17.5	16.9
R_{exp} (%)	3.22	3.17
χ^2	29.7	5.18
R_{Bragg} (%)	31.3	28.6

Elemental analysis – EDXS spectra

Exemplary representative EDXS spectra of primary and recycled LCNC are shown in Figure S5. The measured peaks were assigned to the elements La, Ca, Ni, Cu, and O, which are expected in LCNC. A small amount of Si impurities might be present. This could originate from the ball mill, which was cleaned with quartz sand. Carbon peaks were present in some of the spectra due to the utilisation of conductive tape. No other peaks from impurity elements were detected in any of the samples.
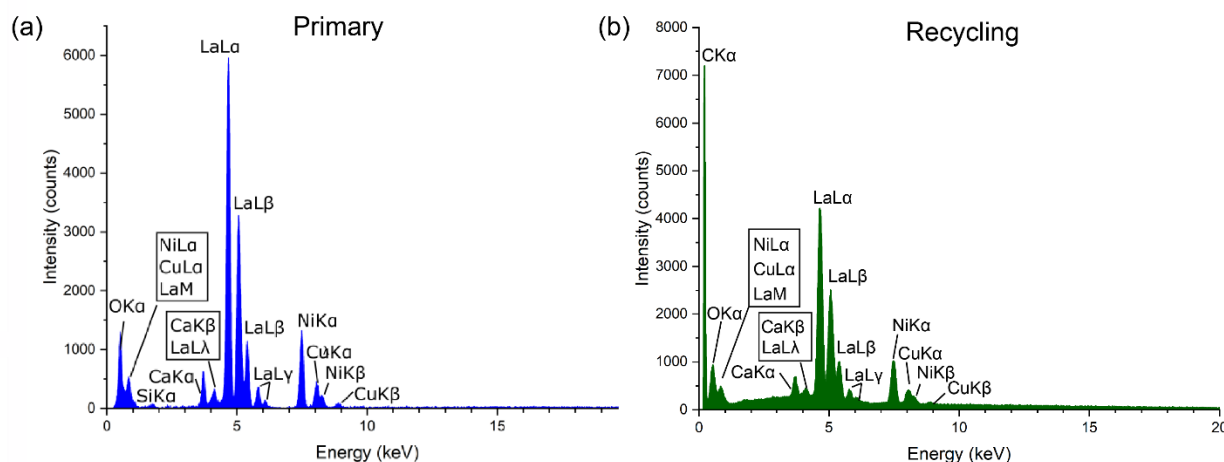
Figure S5: Exemplary EDXS spectrum measured for a primary (a) and recycled (b) LCNC powder sample. Peaks were assigned to the respective elements.

Thermal analysis

Phase analysis

The successful reaction of primary and recycled precursor gels into LCNC during the thermal analysis was confirmed by PXRD. The XRD patterns after thermal analysis in Figure S6 are comparable to their respective reference pattern after the regular synthesis of LCNC powder.

Figure S6: XRD pattern of primary (a) and recycled (b) samples after TG-DTA measurement up to 1100 °C compared to calcined reference samples. Theoretical reflections of a reference material with K_2NiF_4-type structure (COD 96-153-2374) are provided as reference.

Phase formation temperature

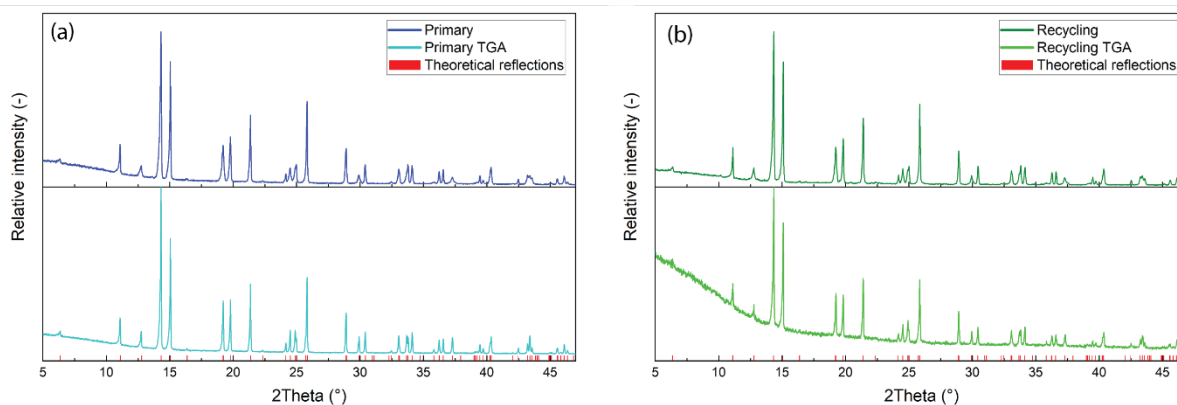The broad, slightly exothermic peak just below 600 °C measured in TG-DTA of primary and recycled samples could arise from the phase formation or from a final combustion of remaining organics. To test its origin in phase formation, TG-DTA of another primary gel was stopped at 600 °C. Up to 600 °C, a similar reaction behaviour as in Figure 5 was observed. PXRD was conducted directly after the measurement and after subsequent annealing of the sample at 600 °C for 10 h. The results are shown in Figure S7 compared to a reference pattern from the same batch.

The XRD pattern after thermal analysis shows the emerging of LCNC's characteristic diffraction peaks, but no explicit peaks. The intensity of the characteristic reflections further increased after annealing of the sample. Hence, the phase formation at around 600 °C is confirmed. However, a longer reaction time or higher temperatures would be needed to obtain crystalline samples. Based on the results, the slight positive weight change above 600 °C could originate from the ongoing reaction of metal ions with oxygen to form the oxide LCNC. A direct phase formation from the precursor is indicated by the emerging of the characteristic reflections at 600 °C. However, potentially low crystallinity of intermediate phases, which would make the diffraction peaks disappear in the high background, prevents a full judgement on the phase formation process.
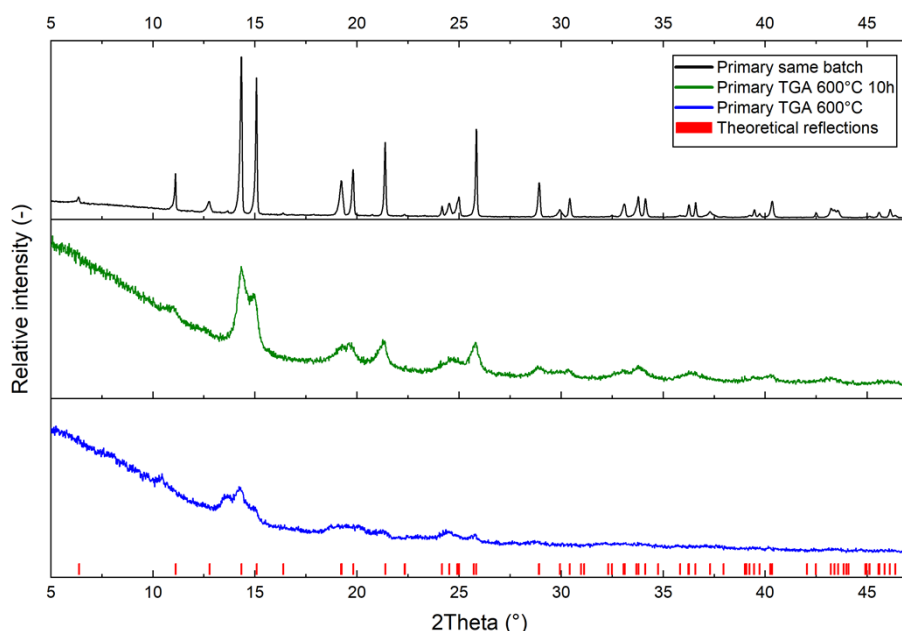
Figure S7: XRD patterns of LCNC precursor gel measured in TG-DTA up to 600 °C directly after analysis and after further annealing at 600 °C for 10 h compared to a reference pattern of LCNC synthesised from the same batch.

Identification of process emissions by TG-MS-FTIR

The relevant process emissions during the pre-calcination and calcination of primary and recycled LCNC precursor gels were identified by combined TG-DTA, MS, and FTIR. The general thermal behaviour in TG-DTA up to the maximum temperature of 800 °C was similar to the measurements shown in Figure 5 (see Figure S8 and Figure S9). The different steps of the reaction behaviour are also visible in the TG-MS and TG-FTIR curves of both samples (see Figure S10 to Figure S13). The emission spectra were divided into the two temperature ranges of pre-calcination (< 350 °C) and calcination (> 350 °C). Due to the similar behaviour of primary and recycled samples, the results are jointly presented and discussed.
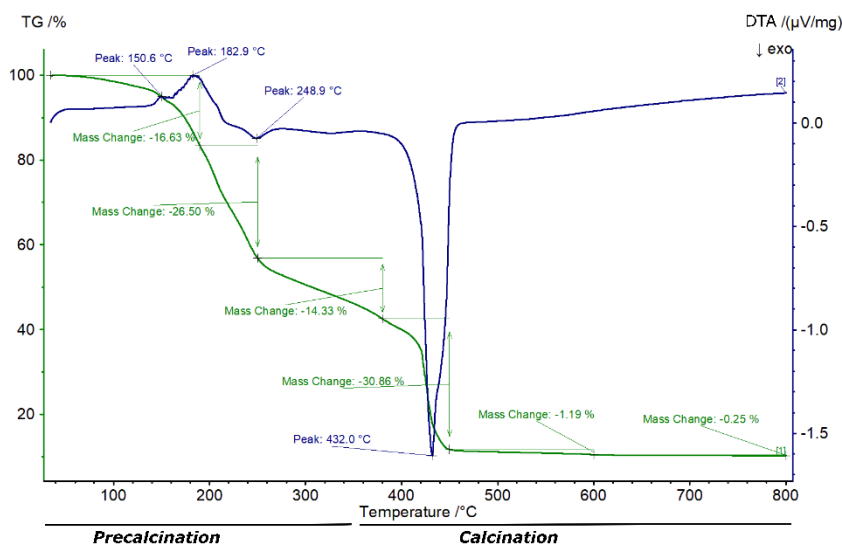
Figure S8: Results of TG-DTA during TG-MS and TG-FTIR measurement of a primary precursor gel. The measurement was conducted between room temperature and 800 °C with a heating rate of 3 K min^{-1} using compressed synthetic air (40 mL min^{-1}) as reactive gas and nitrogen (20 mL min^{-1}) as protective gas.
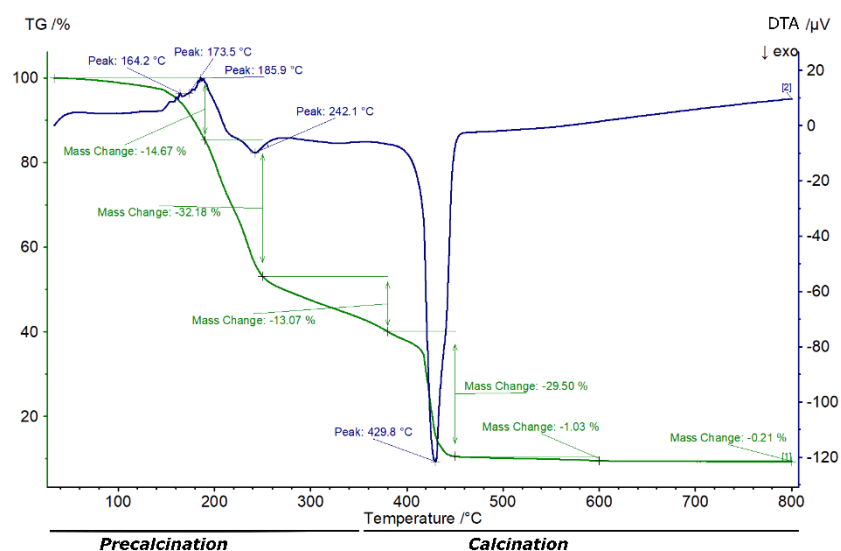
Figure S9: Results of TG-DTA during TG-MS and TG-FTIR measurement of a recycled precursor gel. The measurement was conducted between room temperature and 800 °C with a heating rate of 3 K min^{-1} using compressed synthetic air (40 mL min^{-1}) as reactive gas and nitrogen (20 mL min^{-1}) as protective gas.

The gas species identified by MS are listed in Table S3 along with their primary and secondary signals. The identity of emissions was confirmed by analysing the FTIR absorption intensity in dependence on the temperature for characteristic bands of selected species (see Table S4). The gas species were assigned to the relevant temperature ranges by the combined interpretation of MS and FTIR results as discussed in the following. The relevant MS signals are presented in Figure S10 and Figure S11 for primary and recycled samples, respectively. Due to the overlap of MS signals for various species, the TG-FTIR are presented as complementary information (see Figure S12 and Figure S13).

Table S3: List of identified emitted gas species with their respective primary and secondary MS signals. The applicable temperature range was derived from MS and FTIR data. (DL: detection limit)

Gas species	Primary signal Mass-charge ratio m/z	Secondary signals Mass-charge ratio m/z	Pre-calcination <350 °C	Calcination >350 °C
NO	30	16, 14	Yes	Yes
NO_2	46	30, 16, 14	No	Yes
N_2O	44	30, 28, 16, 14	Yes	Yes
NH_3	17	16, 15, 14, 1	Yes	Yes
CO_2	44	28, 16, 12; 45 (isotope)	Yes	Yes
CO	28	16, 12	Yes	Yes
HNCO	43	42, 29, 28, 15 [16]	Close to DL	No
C_2NH_3	41	40, 39, 38, 14 [17]	Close to DL	Close to DL
CH_4	16	12, 2, 1	Unclear	Unclear
H_2O	18	18, 17, 2 ,1	Yes	Yes
O_2	32	16	Unclear	Input

Table S4: Selected characteristic absorption bands of relevant species that require FTIR for identification.

Gas species	Characteristic absorption band ranges (cm^{-1})	Source
NO	1910-1887, 1848-1810	[18]
N_2O	2253-2227, 2222-2185, 1282-1257, 594-586	[19]
NH_3	3339-3331, 1632-1622, 968-959, 934-926	[20]
CO_2	2378-2316	[21]
CO	2116-2094, 2191-2164	[22]
CH_4	3019-3011, 1307-1301	[23]
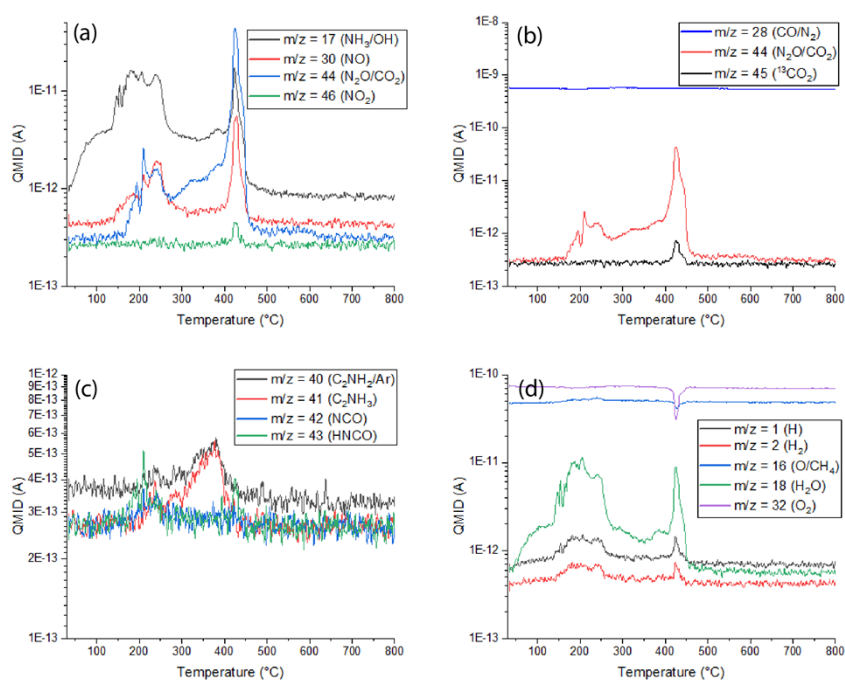
Figure S10: Measured QMID (quasi multiple ion detection) during thermal analysis of a primary LCNC precursor gel for nitrogen-containing species (a), carbon-containing species (b), larger fragments (c), and hydrogen- and oxygen-containing species (d). Assignment of signals to the categories is not unambiguous due to the overlap of MS signals.

Figure S11: Measured QMID (quasi multiple ion detection) during thermal analysis of a recycled LCNC precursor gel for nitrogen-containing species (a), carbon-containing species (b), larger fragments (c), and hydrogen- and oxygen-containing species (d). Assignment of signals to the categories is not unambiguous due to the overlap of MS signals.

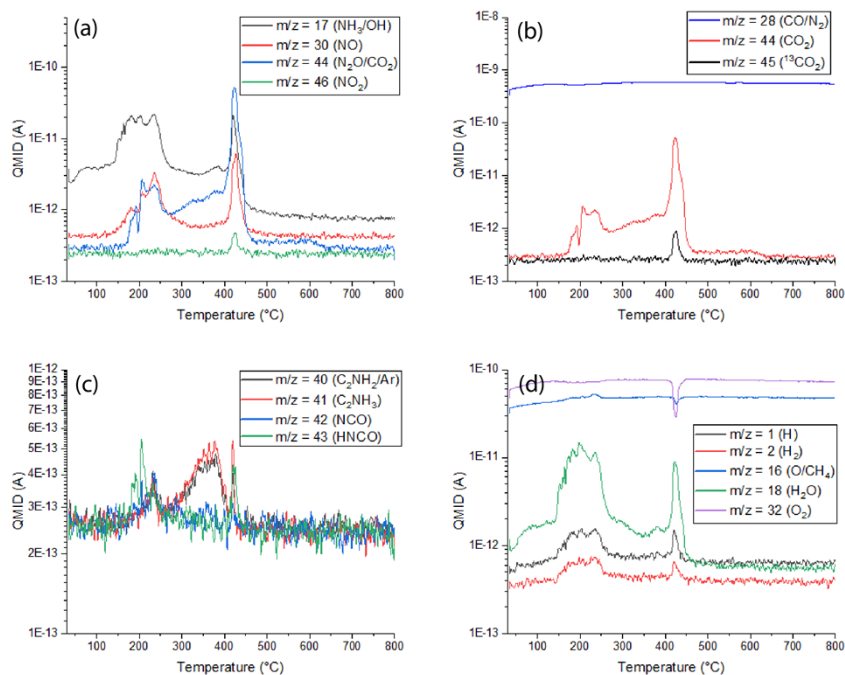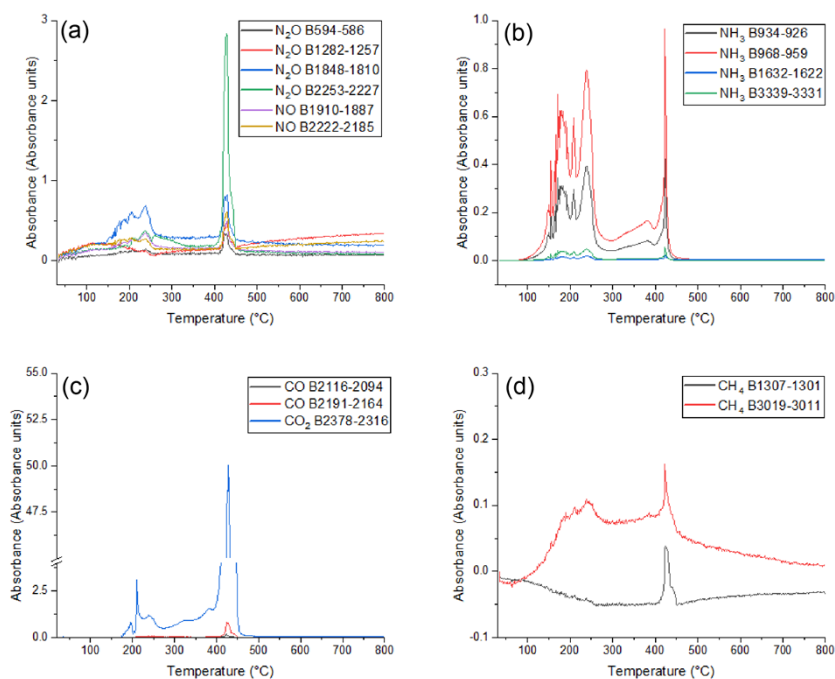
Figure S12: FTIR absorbance during thermal analysis of a primary LCNC precursor gel for selected bands of relevant nitrogen-containing species (a, b), carbon oxides (c), and methane (d).
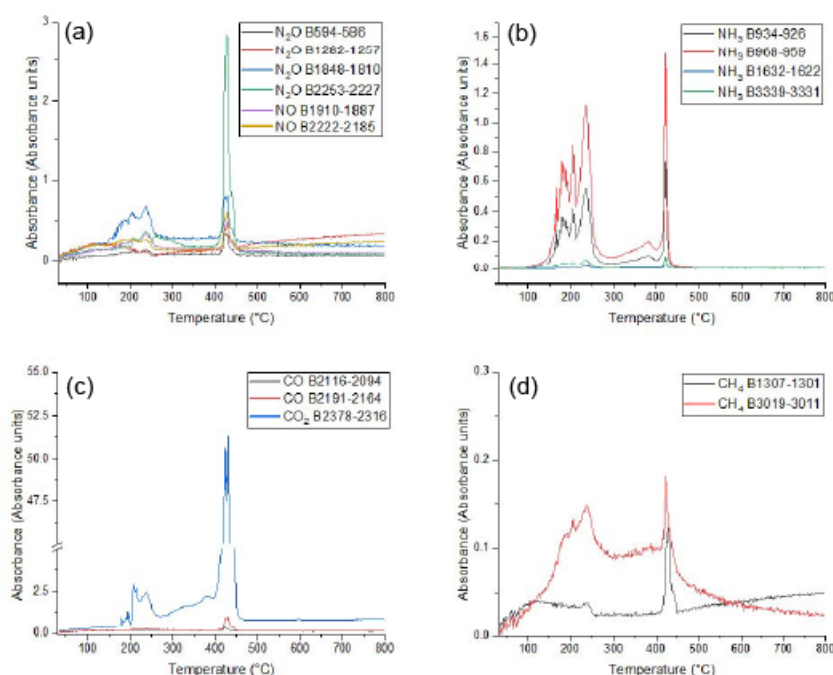
Figure S13: FTIR absorbance during thermal analysis of a recycled LCNC precursor gel for selected bands of relevant nitrogen-containing species (a, b), carbon oxides (c), and methane (d).

Different nitrogen-containing species were detected in both temperature ranges. Due to the large N_2 content in air, potential primary MS signals from N_2 and CO emissions (m/z of 28) are below the detection limit. NO_2 is identified by the MS signal at m/z of 46 at around 420 °C. For NO, the signal at m/z of 30 is the primary signal. It might also originate from NO_2 splitting. However, it is also present below 350 °C and the evolution of NO is confirmed by the FTIR signals. N_2O emissions are identified in both temperature ranges by the simultaneous signal evolution for different FTIR bands. The potential MS signal of N_2O at m/z of 44 overlaps with the signal of CO_2. The emission of NH_3 is also confirmed by the FTIR results. With a m/z ratio of 17 for NH_3, the primary MS signal overlaps with the secondary signal of water from OH.

Emissions of CO_2 and CO were detected at both reaction stages with a much higher peak during the calcination. Due to overlaps of both MS signals with other species, the FTIR analysis is needed for interpretation. The FTIR bands show a smaller peak during pre-calcination and larger peak during calcination. The FTIR signal for CO_2 indicates that a large share of the MS signal at m/z of 44 originates from CO_2 due to the high intensity and similar curve progression. The MS signal for the $^{13}CO_2$ isotope (m/z = 45) further confirms the high amount of CO_2 emissions during calcination. Below 350 °C, the emissions of $^{13}CO_2$ are below the MS detection limit due to the small share of ^{13}C and lower emissions.

No large organic fragments of free CA or EDTA were detected. However, they might have high ionization energies and therefore pass the MS without detection or be split into smaller fragments. Such organic fragments show signals close to the detection limit of MS at m/z between 40 and 43. They are most likely assigned to HNCO and C_2NH_3. The small peaks for C_2NH_3 at around 350 °C and HNCO at around 200 °C could originate from the direct emission of EDTA and splitting in the detector or decomposition of EDTA in the precursor gel. Despite the potential overlap of the m/z 40 signal with the signal of argon, the similar progression of the primary and secondary curve of C_2NH_3 indicates a detection. The FTIR signals for CH_4 bands might also suggest a small share of CH_4 emissions. However, the two curves do not evolve in parallel for the primary sample. The MS signal at m/z of 16 overlaps with the signal of oxygen and the curve thus does not provide further information.

The emission of water starts well below 100 °C according to the primary and secondary MS signals. The continuous emission of water can be assigned to the evaporation of residual solvent and water vapor formed as a reaction product.

The MS signal for oxygen molecules and the secondary signal for oxygen atoms show a different behaviour than the other curves. At ~ 410 °C, a negative peak is detected. This can most likely be assigned to the consumption of oxygen from air during the calcination reaction. However, it could also originate from dilution of oxygen in the reaction atmosphere due to the large amount of other emitted gasses in this temperature range. If significant dilution occurs, the baseline of nitrogen and argon signals should be affected as well. A closer look into the MS signal of N_2 does not show an intensity decrease but slight increase at the relevant temperature range. Therefore, the negative peak in the oxygen signal is mainly caused by the consumption of oxygen.

The summarised results of the emission analysis in Table S3 are consistent with the general reaction behaviour. The results were used to build the emission model for life cycle assessment (see below). The potential emissions of larger fragments and methane were neglected for simplicity reasons as they are close to the detection limit. Note that no quantification of emissions is possible from the obtained results. Quantification by MS or FTIR would require extensive calibration work which was not conducted in this study.

Oxygen transport membrane examination

LCNC membrane discs from primary and recycled LCNC powder were subjected to membrane characterisation to compare the membrane morphology, phase structure, and density.

The XRD results for membranes produced from primary and recycled LCNC displayed in Figure S14 show a similar pattern for both membranes. All reflections of LCNC powder (K_2NiF_4-type structure) are also visible in the diffraction patters of sintered bulk measured in reflection mode. The background is much lower than in transmission mode due to the direct measurement of the sample without any amorphous foil. No additional reflections from impurity phases are visible in the pattern. Hence, LCNC is stable at 1050 °C and the Ruddlesden-Popper phase is retained during sintering.

The membrane surfaces and cross sections were investigated by SEM to check the origin of high leakage and compare the primary and recycled discs (see Figure S15 and Figure S16). The images were obtained after the permeation measurement in case of recycled samples. The high porosity and insufficient sintering of the membranes are clearly visible.
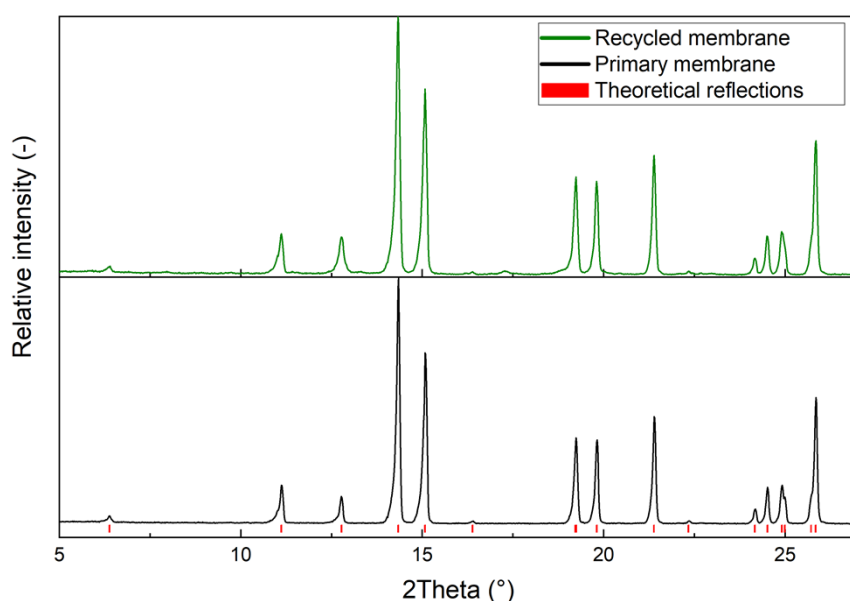

Figure S14: XRD patterns of LCNC membranes from primary and recycled powder measured in reflection mode after sintering at 1050 °C for 20 h.

Both sample types show a very similar microstructure. Traces from cutting and grinding are visible on both samples. The cross section and surface of both membranes have areas with open porosity and weakly connected grains. Pores with a size in the μm-range are visible in both samples. In other areas of the samples, a grain structure is slightly visible. The grain size is only slightly higher than the particle size of LCNC powder.

Besides a high porosity, the leakage could also originate from improper connection of the membrane and the alumina tube. However, the glued edge in Figure S16 shows a tight connection of the membrane with the alumina tube. This makes the porosity of the sample most likely the main contributor to the high leakage flux of ~80 % during the permeation measurement.

The results of membrane characterisation clearly reveal that the chosen sintering parameters are not suitable for the production of high quality LCNC membranes. The high open porosity and low density could have several origins.

(1) The sintering temperature of 1050 °C is not suitable for sintering of LCNC.

(2) The sintering time is not sufficient for good densification and particle growth.

(3) The LCNC powder shows strong interconnection of the particles after calcination. This could hinder pressing of dense green bodies.

Literature examples on $La_2NiO_{4+\delta}$ report sintering conditions of 1350 °C for 10 h (2 K min⁻¹) [24] and 1300 °C for 24 h [25] to obtain sufficiently dense membranes. The values suggest higher sintering temperatures and lower heating and cooling rates. However, parameters for $La_2NiO_{4+\delta}$ might not be transferable to LCNC directly due to the substitution with Ca and Cu. Therefore, systematic sintering studies should be performed to find suitable conditions for pressing and sintering of LCNC.

The comparison of membranes from primary and recycled LCNC shows very similar sintering behaviour. The results thus support the performance equivalence despite the general need for membrane improvement. Functional oxygen transport membranes should be gas tight to enable selective oxygen transport. For this manner, > 95 % rel. Archimedes density have been reported as a general requirement [26]. The measured sample achieves such high value, but open porosity is not indicated by the Archimedes principle. Therefore, the geometrical density should be taken as an additional quality indicator in future sintering studies.
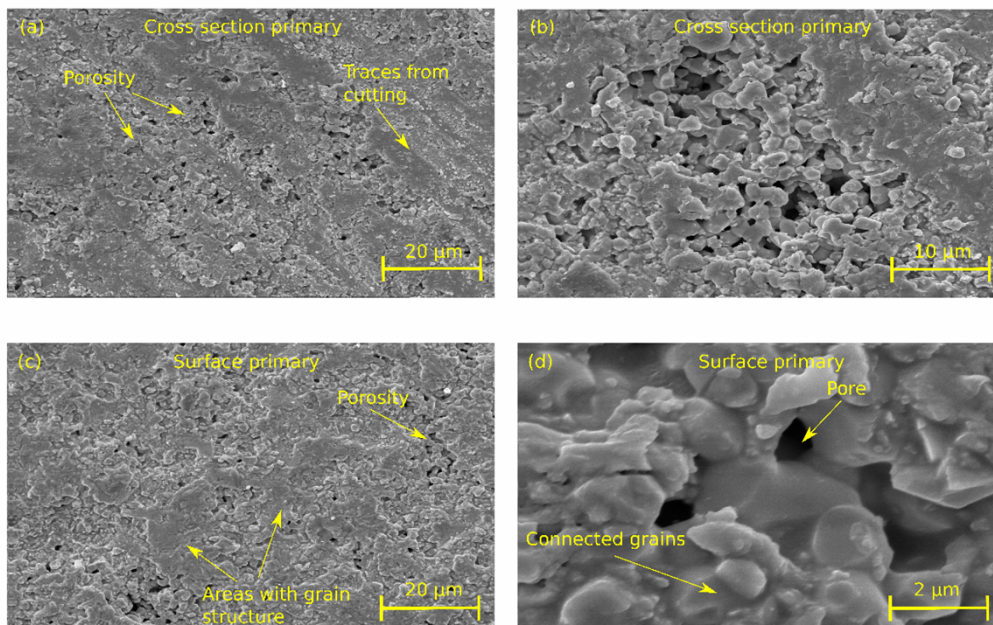
Figure S15: SEM images of the cross section (a, b) and surface (c, d) of membranes produced from primary LCNC in different magnifications.
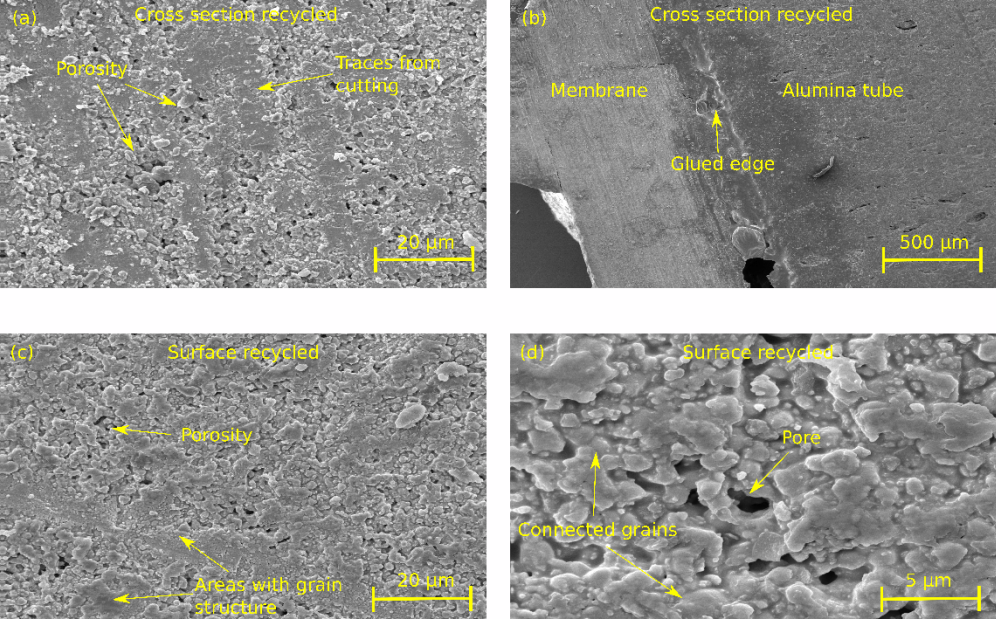
Figure S16: SEM images of the cross section (a, b) and surface (c, d) of membranes produced from recycled LCNC in different magnifications.

Methodology remarks on life cycle assessment (LCA)

An attributional LCA model using the cut-off approach was chosen in consideration of the LCA goal. This enabled the assessment of the environmental impacts (EIs) from primary synthesis (1) and recycling (2) separately, but in a comparable, consistent manner. By choosing a cut-off approach, the production of primary and recycled LCNC were treated as independent first and second life cycle of the material. The EI from the recycling treatment, but not the primary production, was assigned to the production of recycled LCNC. Additional end-of-life treatment of membranes in case of future application was not considered in the current study, where primary LCNC powder was recycled directly.

The cradle-to-gate systems for the LCNC primary synthesis (1) and recycling (2) were derived from the sub-process steps (see Figure 2, main text). Upstream processes included the production and provision of reactants, process chemicals, and electricity. Foreground data was collected for the respective synthesis process and additional dissolution in case of recycling. Process emissions are directly released as elementary flows into the ecosphere. The assessed synthesis does not produce any chemical waste from the chemical reaction itself. However, the measured loss of metal ions was considered as emissions for consistency.
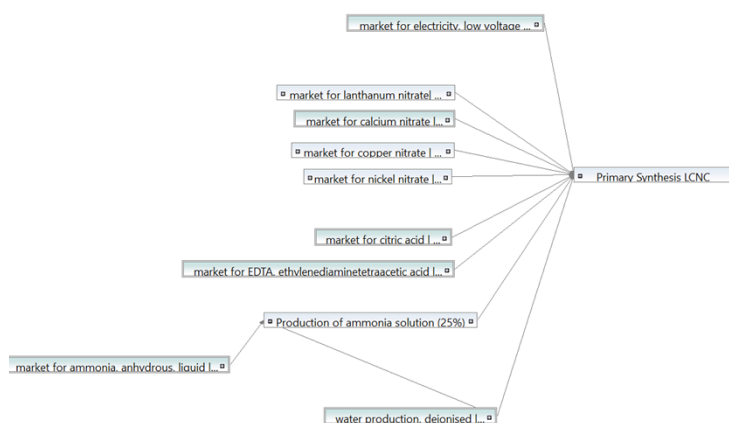
Figure S17: Model graph in OpenLCA for primary synthesis of LCNC. Background processes of nitrate production are not fully expanded for clearer arrangement.
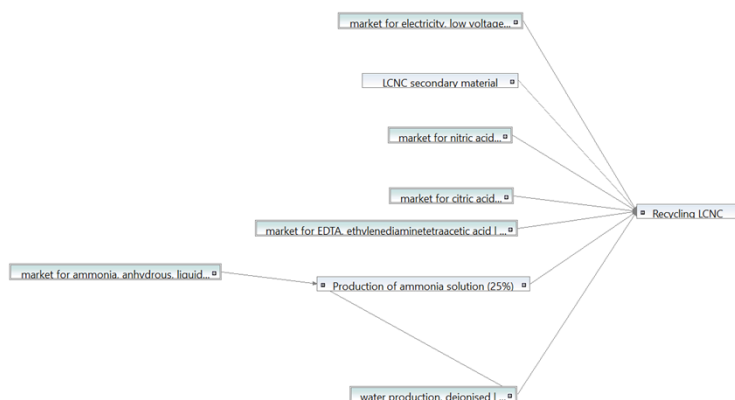
Figure S18: Model graph in OpenLCA for recycling of LCNC. No further background processes were modelled.

The modelled product systems in openLCA [27] are shown in Figure S17 and Figure S18 for the primary synthesis (1) and recycling (2), respectively. The final life cycle inventory (LCI) was accumulated for the overall primary synthesis or recycling as one unit process. The sub-process steps were not evaluated separately. This ensured feasibility to develop an emission model which maintains the overall mass and atomic balance with scientific-based assumptions. The approach also facilitated the evaluation of the influence of up-stream processes in comparison to the foreground process. The input flows from background processes were modelled in OpenLCA by external average process data and modified processes from ecoinvent 3.8 [28] as background data.

Life cycle inventory model

The data structure for obtaining a full life cycle inventory (LCI) of the product systems is summarised in Table S5. Due to the similar modelling approach for the same flow category (e.g., process chemicals, electricity) at all process stages and in both product systems, the flow category was chosen to structure the presentation of the data model. The flow categories were classified as product, waste, or elementary flow. Input and output flows were also distinguished.

Table S5: Overview of data structure and modelling approach for the considered flow categories. Quantification in the foreground system by primary data and modelling of the background data using ecoinvent 3.8 database [28] are briefly described.

Flow category	Flow type	Primary data input	Background data modelling	Background process type
Source of environmental impact	*Classification / Input or output*	*Measured or theoretical data input for 5 g metal ion batch*	*Approach for modelling of background system*	*Specification of process type in OpenLCA*
Chemical reactants (metal nitrates)	Product / Input	Mass per reactant (g)	Process incl. production and market of chemical reactants in Europe/globally	System process: $Ca(NO_3)_2$ Modified unit processes: $La(NO_3)_3$, $Cu(NO_3)_2$, $Ni(NO_3)_2$
Chemical reactant (secondary LCNC powder)	Recyclable material / Input	Mass of LCNC (g)	Burden-free due to cut-off	n/a
Process chemicals (all except metal nitrates)	Product / Input	Mass per process chemical (g)	Process incl. production and market of process chemicals in Europe/globally	System processes: CA, EDTA, nitric acid Modified unit process: Ammonia solution (25%)
Electricity	Product / Input	Consumed electricity (kWh)	Process incl. production and market of low voltage electricity in Germany	System process
Oxygen from air	Elementary / Input	Mass of oxygen deficit for reaction (g) - *theoretical model*	Elementary flow - no background process	n/a
Process emissions to air	Elementary / Output	Mass of emitted gasses per type (g) - *theoretical model*	Elementary flow - no background process	n/a
Process emissions to water	Elementary / Output	Mass of metal ion loss per type to water (g) - *theoretical model*	Elementary flow - no background process	n/a

Primary data

The input and output flows of the synthesis process were measured as primary data as described in Table S6 or modelled using a specific emission model. Three individual data sets were collected for each system. In general, the average of three batches was calculated for the final LCI value of each system. For the steps of pre-calcination, ball milling, and calcination, the electricity consumption of both systems should be identical. Therefore, the average of all available data sets was taken for both systems to avoid distortion. Exceptions are detailed in the following. The third data point for electricity consumption during calcination was obtained for a furnace of doubled size compared to previous data sets. The utilization of a larger furnace results in almost doubled electricity consumption and therefore increases the standard deviation. Furthermore, the third data set for primary synthesis misses one flow for the electricity consumption during pre-calcination. These factors have no influence on the comparison of the two product systems. The same average data from all data sets was used in both systems for pre-calcination, ball milling, and calcination. The data for electricity consumption during gelation in primary synthesis had one massive outlier with almost doubled consumption. This most likely originated from experimental errors and lead to unreasonable higher electricity consumption for the primary synthesis. The data point was thus excluded from the mean value.

In a next step, the average flows were scaled to 1 g LCNC powder. The presented standard deviations in the LCI (see Table S10 and S11) provide an estimate of data uncertainty for primary data. The foreground data reflects the material and electricity consumption as well as emissions at laboratory scale as accurate as possible. This results in a high geographical, temporal, and technological representativeness for the processing conditions at laboratory scale. The emission model was also based on generic literature data to estimate the emission shares. Therefore, the overall specificity for the emissions and oxygen consumption is only moderate.

Table S6: Overview of collected primary data of product systems (1) and (2). Measured flows connect the processes of background and foreground system or the sub-processes of the foreground system with each other.

Flow	Connection Input from / Output to	Data collection approach	Sub-process and product system
Electricity	Background/ Foreground	Plug-in electricity meter Voltcraft SEM 4500 (kWh)	All except dissolution EDTA (1,2) and preparation of ammonia solution (1,2)
Metal nitrates (individually)	Background/ Foreground	Weighing (g)	Dissolution Nitrates (1)
Citric acid	Background/ Foreground	Weighing (g)	Dissolution Nitrates (1)/ Dissolution LCNC (2)
EDTA	Background/ Foreground	Weighing (g)	Dissolution EDTA (1,2)
Ammonia solution (25%)	Background/ Foreground	Measuring cylinder (mL)	Preparation of ammonia solution (1,2)
Nitric acid	Background/ Foreground	Automatic pipet (mL)	Dissolution LCNC (2)
Deionised water	Background/ Foreground	Measuring cylinder (mL)	Dissolution Nitrates (1)/ Dissolution LCNC (2), Preparation of ammonia solution (1,2)
LCNC powder	Foreground/ n/a	Weighing (g)	Calcination (1,2)

Background processes

The provider processes were taken from the ecoinvent database directly or as modified versions of ecoinvent processes (see below). Hence, the specificity of their input and output flows is classified as low. Provider processes are based on average data and deviations in transport distances, processing effort due to chemical purity, different processing technology, and others are expected. Future technological developments, e.g., 100 % renewable energies, were not considered. The background

processes were selected to be most representative for the synthesis in Germany, where the CO_2 plasma technology is currently developed. If LCI data for average background processes was not available (i.e., for certain metal nitrates), comparable ecoinvent processes were modified.

Process chemicals

All utilised background processes for process chemicals are listed in Table S7. Background processes for the production and provision of the process chemicals citric acid (CA), EDTA, deionised water (DI water), and nitric acid (only system (2)) were directly taken from the ecoinvent 3.8 database [28]. Average market processes were selected as system processes with the highest possible representativeness. Because DI water was produced on site, only its production was considered.

For the production of ammonia solution (25 %), a new process was created. Selected providers for input flows are the market for liquid ammonia and production of DI water. The weight ratio of the ammonia and DI-water flow is 1:3. A second market process for the produced ammonia solution (25 %) was not included.
For the utilised chemicals, no specific information regarding the production technology and location is currently available from the manufacturers. This lack of specific information on geographical and technological product origin potentially limits the data representativeness. Due to the use of reaction grade chemicals in the experimental study, the selected processes might underestimate the processing effort. However, the lack of information does currently not allow more precise modelling. The related uncertainties and discrepancies apply equally to both product systems in the case of CA, EDTA, DI water, and ammonia solution. Nitric acid is only used in system (2). The data uncertainty for the production and provision of metal nitrates applies only to system (1).

Table S7: Background processes for production and provision of process chemicals taken from ecoinvent 3.8 database [28].

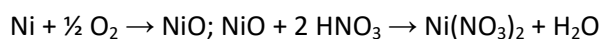| Process chemical	Ecoinvent process category Type/ Framework/ Location	Process name	Process number
Citric acid	Market/ System process/ Global	market for citric acid	citric acid	Cutoff, S	7039c244–7360–38b5–a8c0–6fd406a0ae7e
EDTA	Market/ System process/ Global	market for EDTA, ethylenediaminetetraacetic acid	EDTA, ethylenediaminetetraacetic acid	Cutoff, S	d70aed1f–add6–3f5c–8674–d1185dd1f61c
Deionised water	Production/ System process/ Europe without Switzerland	water production, deionised	water, deionised	Cutoff, S	e08c08c5–88cd–4581–8523–42b0b66853d3
Nitric acid	Market/ System process/ Europe without Russia	market for nitric acid, without water, in 50% solution state	nitric acid, without water, in 50% solution state	Cutoff, S	8b2c9828–aef7–4d83–98ed–8d2eafe58e63
Ammonia solution (25%)	Production/ Created process	Production of ammonia solution (25%)	Cutoff, U	n/a
Input for ammonia solution (25%)	Market/ System process/ Europe	market for ammonia, anhydrous, liquid	ammonia, anhydrous, liquid	Cutoff, S	d9f39a29–fe56–390c–afc9–6057cc7b3ca7
Input for ammonia solution (25%)	Production/ System process/ Europe without Switzerland	water production, deionised	water, deionised	Cutoff, S	e08c08c5–88cd–4581–8523–42b0b66853d3

Metal nitrates

The reactants lanthanum nitrate, calcium nitrate, nickel nitrate, and copper nitrate are only input materials for the primary synthesis of LCNC (1). They are referred to as metal nitrates in the following. The utilised processes are listed in Table S8. In the ecoinvent database, processes are currently only available for the production and market of calcium nitrate [28]. As provider of calcium nitrate, the European system process for the market of calcium nitrate was selected. The production and market processes for the other three metal nitrates were modelled by modifying processes of related chemicals with similar processing pathways.
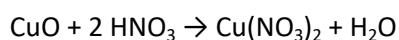
Due to the similar production methods, available unit processes for production of metal sulphates were modified. In the production of metal sulphates, metal oxides are dissolved in sulphuric acid [29,30]. Similarly, they are dissolved in nitric acid for the production of metal nitrates [30–33].

To model the production of nickel nitrate and copper nitrate, unit processes for nickel sulphate production and copper sulphate production were modified, respectively. Sulphuric acid was exchanged by nitric acid as input material. The required inputs of nitric acid and elemental nickel or copper oxide were calculated for the production of 1 kg nitrate according to the respective reaction equations:

Production of nickel nitrate:

$Ni + ½ O_2 \rightarrow NiO$; $NiO + 2 HNO_3 \rightarrow Ni(NO_3)_2 + H_2O$

Production of copper nitrate:

$CuO + 2 HNO_3 \rightarrow Cu(NO_3)_2 + H_2O$

To directly enable the utilisation of the measured metal nitrate mass, the necessary amount of crystal water was added as input of DI water and considered in the product output. The basic process in ecoinvent does not consider differences in the processing steps due to varying amounts of crystal water. Sulphur emissions were removed in the output flows.

An average of 0.53 % metal ion emissions with respect to the total metal ion input is included in the reference processes of metal sulphate production. This percentage was added as metal ion emission to the modified processes. The respective additional metal oxide input was added to keep the atomic balance of the metal ions. The providers of all input materials for the nitrate production were exchanged to system processes as they were not investigated in detail.

For the modelling of market processes, nickel sulphate and copper sulphate were exchanged by nickel nitrate and copper nitrate in the available market processes. The modified production processes described above were selected as providers.

In the case of lanthanum nitrate, no process for production of lanthanum sulphate is currently available in the database [28]. Therefore, the newly modelled process for production of copper nitrate was further modified. Copper oxide was replaced by lanthanum oxide. The mass of lanthanum oxide and nitric acid was adjusted according to the following reaction equation.

Production of lanthanum nitrate:

$La_2O_3 + 6 HNO_3 \rightarrow 2 La(NO_3)_3 + 3 H_2O$
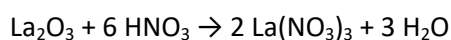
Similarly, the required amount of crystal water to produce $La(NO_3)_3 \cdot 6 H_2O$ was included. Emissions of copper were exchanged by a flow of lanthanum emissions equal to 0.53 % of La-ions in the product. The respective amount of La_2O_3 was added as additional input.

To model the market process for lanthanum nitrate, the created market process for copper nitrate was modified. Copper nitrate was exchanged by lanthanum nitrate.

Table S8: Processes from ecoinvent 3.8 [28] used in the background system for the production and provision of the metal nitrates. The input processes for process modifications are listed as well.

Reactant	Process modification	Ecoinvent category Type/ Framework/ Location	Original process	Process number	Modified process
Calcium nitrate	Original	Market/ System process/ Europe	market for calcium nitrate | calcium nitrate | Cutoff, S	b1c5aa62–b8cb–4a66–9dde–842663decfe1	n/a
Nickel nitrate	Modified	Production/ Unit process/ Global	nickel sulfate production | nickel sulfate | Cutoff, U	19794dfa–e861–3740–bd8b–66b200dde694	nickel nitrate production | modified nickel sulfate | Cutoff, U
Nickel nitrate	Modified	Market/ Unit process/ Global	market for nickel sulfate | nickel sulfate | Cutoff, U	a763c67b–f3bf–35f4–acd5–acae3825eb79	market for nickel nitrate | modified nickel sulfate | Cutoff, U
Copper nitrate	Modified	Production/ Unit process/ Global	copper sulfate production | copper sulfate | Cutoff, U	790ed9ee–bf19–32e2–b93a–ca0e9c0b5d14	copper nitrate production | modified copper sulfate | Cutoff, U
Copper nitrate	Modified	Market/ Unit process/ Global	market for copper sulfate | copper sulfate | Cutoff, U	329e8d72–9c2b–362a–88ac–5dc9d0e1bba8	market for copper nitrate | modified copper sulfate | Cutoff, U
Lanthanum nitrate	Modified	Production/ Unit process/ Global	copper sulfate production | copper sulfate | Cutoff, U	790ed9ee–bf19–32e2–b93a–ca0e9c0b5d14	lanthanum nitrate production | modified copper sulfate | Cutoff, U
Lanthanum nitrate	Modified	Market/ Unit process/ Global	market for copper sulfate | copper sulfate | Cutoff, U	329e8d72–9c2b–362a–88ac–5dc9d0e1bba8	market for lanthanum nitrate| modified copper sulfate | Cutoff, U
Lanthanum oxide	Input for modified	Market/ System process/ Global	market for lanthanum oxide | lanthanum oxide | Cutoff, S	052c379d–f23f–389c–9c7e–d71b100f1106	n/a
Nitric acid	Input for modified	Market/ System process/ Europe without Russia	market for nitric acid, without water, in 50% solution state | nitric acid, without water, in 50% solution state | Cutoff, S	8b2c9828–aef7–4d83–98ed–8d2eafe58e63	n/a

Emission model for process emissions

The Pechini-based process causes a significant amount of different carbon- and nitrogen-containing process emissions. The process is based on the formation of a metal-organic precursor gel and subsequent removal of organics during pre-calcination and calcination. The organic part of the precursor reacts with nitrate ions and oxygen into gaseous process emissions. The metal ions react with oxygen into LCNC. The consumed oxygen is provided from the surrounding air.
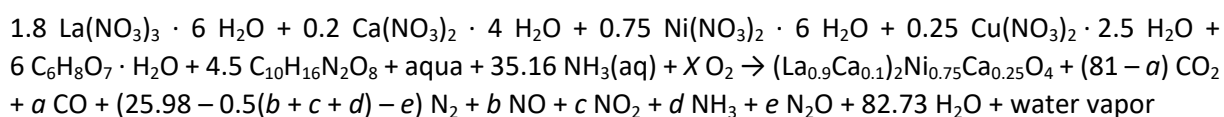
Process emissions can have significant influence on the overall evaluation of synthesis methods. Many LCA studies of sol-gel like processes do not consider the formation of process emissions sufficiently [34–36]. In this work, an emission model was developed to quantify the process emissions for more accurate assessment of the environmental impact (EI). The most relevant gaseous emissions were identified based on MS and FTIR results. The share of emissions was then quantified based on the most representative available literature. In addition to gaseous emissions, loss of metal ions was considered as emissions to water. Emission flows for areas with high population density were selected whenever available. Otherwise, unspecified flows were selected (see LCI).

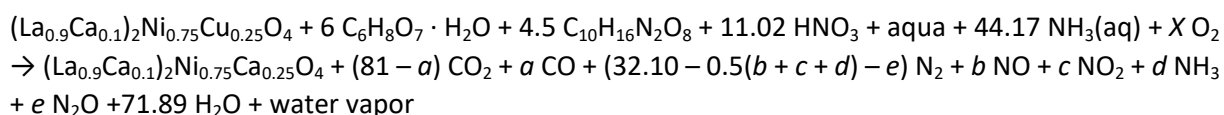<u>Requirements and assumptions</u>

The main requirement for the emission model was to quantity the most contributing process emissions as accurate as possible. It thereby enabled appropriate consideration of process emissions in the overall LCA. Direct measurement of the process emissions was beyond experimental feasibility. Therefore, the emission model had to estimate the expected process emissions based on acquired primary data, results from thermal analysis, and literature. While doing so, the overall theoretical mass and atomic balance of the process must be maintained.

The emission model for gaseous emissions was based on several assumptions to construct a feasible, meaningful emission model with scientific foundation. It was assumed that all organic emissions are emitted as gases to air and all metal ion losses are emitted to water. Further, it was assumed that all chemicals, incl. metal nitrates, have the nominal composition, i.e., also no deviation of crystal water content. Note that small deviations are expected in reality. The emissions with significant contribution were assumed to be identified by combined TG-MS/ TG-FTIR between room temperature and 800 °C. Species with small peak size were considered as negligible. Relevant process emissions were identified as H_2O, CO_2, CO, NH_3, NO, NO_2, and N_2O (see above). The theoretical reaction equation for a complete combustion into LCNC, CO_2 and N_2 is chosen as the basis of the emission model. It is expanded by the additional emissions due to incomplete combustion for primary synthesis and recycling and adjusted to the actual precursor composition as follows.

Primary synthesis:

$$1.8 \text{ La(NO}_3)_3 \cdot 6 \text{ H}_2\text{O} + 0.2 \text{ Ca(NO}_3)_2 \cdot 4 \text{ H}_2\text{O} + 0.75 \text{ Ni(NO}_3)_2 \cdot 6 \text{ H}_2\text{O} + 0.25 \text{ Cu(NO}_3)_2 \cdot 2.5 \text{ H}_2\text{O} + 6 \text{ C}_6\text{H}_8\text{O}_7 \cdot \text{H}_2\text{O} + 4.5 \text{ C}_{10}\text{H}_{16}\text{N}_2\text{O}_8 + \text{aqua} + 35.16 \text{ NH}_3\text{(aq)} + X \text{ O}_2 \rightarrow (\text{La}_{0.9}\text{Ca}_{0.1})_2\text{Ni}_{0.75}\text{Ca}_{0.25}\text{O}_4 + (81 - a) \text{ CO}_2 + a \text{ CO} + (25.98 - 0.5(b + c + d) - e) \text{ N}_2 + b \text{ NO} + c \text{ NO}_2 + d \text{ NH}_3 + e \text{ N}_2\text{O} + 82.73 \text{ H}_2\text{O} + \text{water vapor}$$

Recycling:

$$(\text{La}_{0.9}\text{Ca}_{0.1})_2\text{Ni}_{0.75}\text{Cu}_{0.25}\text{O}_4 + 6 \text{ C}_6\text{H}_8\text{O}_7 \cdot \text{H}_2\text{O} + 4.5 \text{ C}_{10}\text{H}_{16}\text{N}_2\text{O}_8 + 11.02 \text{ HNO}_3 + \text{aqua} + 44.17 \text{ NH}_3\text{(aq)} + X \text{ O}_2 \rightarrow (\text{La}_{0.9}\text{Ca}_{0.1})_2\text{Ni}_{0.75}\text{Ca}_{0.25}\text{O}_4 + (81 - a) \text{ CO}_2 + a \text{ CO} + (32.10 - 0.5(b + c + d) - e) \text{ N}_2 + b \text{ NO} + c \text{ NO}_2 + d \text{ NH}_3 + e \text{ N}_2\text{O} + 71.89 \text{ H}_2\text{O} + \text{water vapor}$$

Due to the reaction in air, unrestricted oxygen exchange was assumed to maintain the atomic balance. The respective amounts of ammonia and nitric acid were calculated based on primary data from the LCI. The reaction products were assessed from the atomic balance. The unknown variables of oxygen consumption X and emission shares a for CO, b for NO, c for NO_2, d for NH_3, and e for N_2O were quantified by the emission model.

The utilised TG-MS/ TG-FTIR method does not enable direct quantification of the variables. Therefore, the best possible estimates based on literature values were used to quantify the emission shares and oxygen consumption. This assumes transferability of the literature results to the given system.

For water and ammonia, it was assumed that the species directly leave the system without further reaction. The evaporation of ammonia from solutions during heating [37] and removal from ammonium nitrate when burning urea ammonium nitrate (UAN) fuel [38] were reported previously. Carbon and remaining nitrogen were assumed to react with oxygen to form CO_x, NO_x, and N_2O. It was assumed that hydrogen from CA and EDTA reacts with oxygen to form water. Specific assumptions on the emission shares are provided in the section on gaseous emissions. The metal ions were assumed to react with oxygen to form LCNC. Material loss was treated as metal ions emitted to water. A loss of other precursor constituents as direct process emissions was not considered.

The reaction behaviour during primary synthesis (1) and recycling (2) is very similar. Hence, identical shares (%) of process emissions, e.g., which share of nitrogen atoms is emitted as NO_2, were assumed for both systems. A difference cannot be fully excluded, since precursor (1) contains nitrate ions from metal nitrates and precursor (2) from nitric acid in a higher amount. However, the measurement results indicate similarity. The chosen approach hence treats the two compared product systems in a consistent manner.

The process emissions were calculated based on average values for the overall reaction. This does not fully reflect the complex nature of the step-wise reaction. However, no well-founded separate quantifications for the sub-processes were possible with the available resources. Furthermore, the total emission balance is most important since all C and N atoms will reach the ecosphere throughout the process. The details of the model are explained in the following sections.

General model framework

The general concept of the emission model is shown in Figure S19. The model is based on the mass and atomic balance for input and output flows. Conversion between measured weight and number of atoms enabled the calculations. The same modelling approach was used for the product systems (1) and (2). However, the calculation of process emissions was adjusted according to the specific input flows (e.g., metal nitrates, nitric acid).
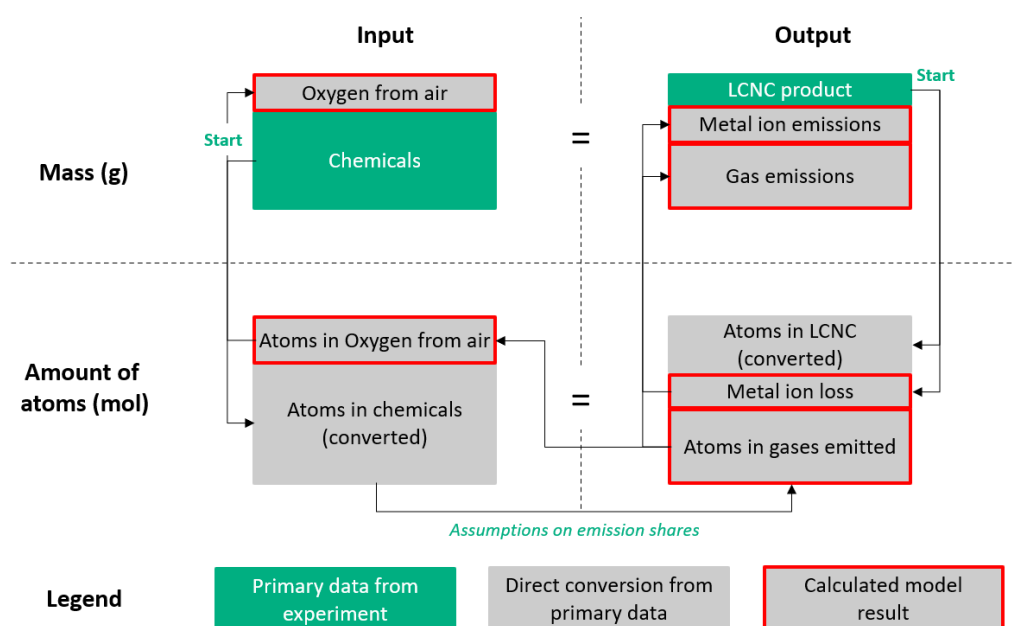

Figure S19: Scheme of the emission model for primary synthesis and recycling of LCNC.

22

The overall mass balance of the process requires that the mass of input chemicals m_{Chem} and oxygen from air m_{O_2} is equal to the mass of produced LCNC m_{LCNC}, the emitted metal ions m_{ions}, and gases m_{gases}.

$$m_{Chem} + m_{O_2} = m_{LCNC} + m_{ions} + m_{gases} \qquad (1)$$

While the mass of chemicals m_{Chem} was known from primary data, the mass of oxygen uptake m_{O_2} remained a variable in the beginning. The measured weight of input chemicals was used to calculate the amount of atoms using the molar mass of their nominal composition. The input of directly emitted species $n_{H_2O}^{in}$ and $n_{NH_3}^{in}$, all metal ions n_{ions}^{in}(La³⁺, Ca²⁺, Ni²⁺, Cu²⁺), oxygen atoms n_O^{in}, carbon n_C^{in}, nitrogen n_N^{in}, and hydrogen n_H^{in} was determined. The input must be equal the output in the emissions and LCNC. The separate atomic balances must also be maintained for each species but are not listed here.

$$\begin{aligned} &n_{ions}^{in} + n_{H_2O}^{in} + n_{NH3}^{in} + n_N^{in} + n_C^{in} + n_H^{in} + n_{O,\,chem}^{in} + n_{O,air}^{in} \\ &= n_{ions}^{LCNC} + n_O^{LCNC} + n_{ions}^{emis} + n_{H_2O}^{emis} + n_{NH_3}^{emis} + n_N^{emis} + n_C^{emis} + n_H^{emis} + n_O^{emis} \end{aligned} \qquad (2)$$

The output of LCNC m_{LCNC} was quantified by weighing during the collection of primary data. This allowed calculation of the number of metal ions n_{ions}^{LCNC} in the produced LCNC. The difference to the theoretical metal ion content of input material was treated as emission of metal ions to water (see below).

The gaseous process emissions were calculated from the amount of all other input chemicals (i.e., excl. metal ions). Each atom must leave the process as part of a process emission. Emissions were separated in H₂O, NH₃, carbon-containing emissions, and other nitrogen-containing emissions. The shares were assigned according to indications from literature (see below). This approach maintains the atomic balance of C, N, and H. Oxygen can be taken from air in this open system to maintain the atomic balance of oxygen. The amount of consumed oxygen $n_{O,air}^{in}$ was calculated by subtracting the amount of oxygen in input materials $n_{O,\,chem}^{in}$ from the amount of oxygen in output gases n_O^{emis} and LCNC n_O^{LCNC}:

$$n_{O,air}^{in} = n_O^{LCNC} + n_O^{emis} - n_{O,\,chem}^{in} \qquad (3)$$

All amounts of emissions and consumed oxygen were converted back into the respective mass using their molar mass. This step delivers the weight of process emissions and consumed oxygen for the LCI.

In order to ensure the consistency of the model, the weight balance (1) and atomic balance (2) were checked. Furthermore, the model also conserves all atoms individually. The mass of calculated emissions except water vapor from DI water was compared to the measured mass change after gelation until the LCNC product was obtained. The deviation is within 6 %. This provides a further plausibility check.

The developed model is partially based on directly measured primary data and theoretical calculations. Hence, the quantified flows do not exactly represent the actual flows during the process on atomic level. Nevertheless, the flows are the best possible estimates of the true input and output flows under the given conditions. Rather than not considering emissions at all, a profound estimation of emissions is important to assess the EI of the Pechini-based synthesis methods in a realistic way.

The following sections describe the modelling of emissions to water and air in more detail.

<u>Emissions to water</u>

Material loss during primary synthesis and recycling was considered as loss of metal ions in the form of emissions to water. In principle, the production of LCNC does not produce waste material for treatment due to its one-pot approach. However, there are two reasons for the deviation of final LCNC output from the theoretically expected output. First, a small fraction of material sticks at the equipment during each process step. Second, the actual metal ion content of metal nitrates in system (1) might deviate from the nominal content due to variation of the water content.

The metal ion emissions were calculated from the difference of the actual LCNC output to the theoretical value of 6.01 g for a batch size of 5 g metal ions. Individual differences for systems (1) and (2) were used. The chosen approach delivers the worst-case value of emissions.

In the first case of material adhesion to equipment, direct emission to water assumes release to the ecosphere during washing of the equipment. In reality, washing water was collected as chemical liquid waste. In later large-scale production, the relative loss is expected to decrease due to larger batch size. In addition, equipment would most likely be used for the same material which could reduce the required extend of washing.

For the primary synthesis (1), the chosen approach is expected to further overestimate the metal ion loss. The complete difference of theoretical and actual output was considered as emissions but the true metal content of metal nitrates might be slightly lower than the theoretical value due to their hygroscopic nature. The exact deviation, however, remained unknown and emissions were considered to maintain the mass balance. This influence of inaccurate stoichiometry has a low contribution. Compared to the theoretical value, the LCNC output was reduced by 5 % for the primary synthesis. A loss of ~3 % can be ascribed to the processing steps as known from recycling.

The newly created flow for La-ions was not considered in the utilised ILCD impact assessment method in openLCA. Therefore, the flow is only listed in the LCI for completeness. No environmental impact was assigned to it.

The chosen model also neglects potential emissions of other precursor constituents such as citric acid, EDTA, and nitric acid to water. These species were assumed to completely react into gaseous process emissions.

Gaseous emissions to air

The gaseous process emissions originate from the evaporation and reactions during gelation, pre-calcination, and calcination. Separate quantification of the process emissions for the different experimental steps was not possible based on the results of thermal analysis and available literature.

The results of thermal analysis clearly reveal the emission of significant amounts of H_2O, NH_3, CO, CO_2, NO, NO_2, and N_2O. The assumed emission shares and sources are listed in Table S9. For simplification, potential emissions of C_2NH_3, $HNCO$, and CH_4 were neglected due to the low expected contribution. In principle, inclusion in future refinements would be possible with the chosen modelling approach.

The following literature was selected to provide information for the quantification. The combustion behaviour and process emissions of urea ammonium nitrate (UAN) fuel were studied in several publications by Grinberg Dana et al. [38–40]. The fuel constituents are comparable to the constituents of LCNC precursors. However, citric acid and EDTA have larger molecular chains than urea. The gel-framework also reacts in two steps. However, a certain extend of transferability of the fuel combustion is expected. Process emissions during glycine nitrate combustion synthesis of different metal oxides

were studied by Pine et al [41]. The study lacks direct comparability because the reaction equation in this work largely deviates from the ratios close to stoichiometric fuel-oxidant ratios in their study [41]. Furthermore, general information on combustion reactions [42] and the Boudouard reaction of coke [43] provided further indications.

Table S9: Emission shares as used in the emission model. Shares were assigned to reference species or atoms for the considered emissions H_2O, NH_3, CO, CO_2, NO, NO_2, and N_2O. The utilised sources are further described in the text.

Reference	Emission	Share of reference	Source
H_2O	H_2O	100 %	n/a
NH_3	NH_3	100 %	Li et al. (2008) [37]; Grinberg Dana et al. (2014) [38]
C	CO	2 %	Boudouard reaction in Holleman Wiberg [43]
C	CO_2	98 %	
N	N_2	0 %	Grinberg Dana et al. (2016) [39]
N	NO	54 %	Grinberg Dana et al. (2014) [38]
N	NO_2	1 %	
N	N_2O	45 %	
H *in reacting chemicals*	H_2O	100 %	n/a

The species H_2O and NH_3 from ammonia solution were assumed to directly leave the system as water vapor and gaseous NH_3. A large fraction of water input evaporates during gelation. Residual water in the gel precursor evaporates during pre-calcination. The high volatility of ammonia suggests that a certain share of ammonia evaporates during gelation as well. For instance, evaporation of ammonia has been used by Li et al. as part of a synthesis process [37]. Furthermore, Grinberg Dana et al. suggested a model for reaction pathways in the combustion of UAN [38]. Formation of NH_3 is suggested as the first step in the reaction of ammonium nitrate. This assumption is transferred to the situation in the precursor: ammonium and nitrate ions are present in the precursor solution and gel. High peaks of ammonia emissions are visible in MS and FTIR spectra. Therefore, direct re-emission of ammonia input was assumed. Formation of ammonia by other reaction pathways was neglected. Because citric acid and EDTA have low volatility, their evaporation during gelation was considered as negligible. Evaporation of nitrate ions during gelation was also neglected.

Carbon-containing emissions of CO and CO_2 were considered in the model. A worst-case estimation of emissions was conducted based on the Boudouard reaction [43]. At a combustion temperature of 450 °C for coke, formation of 2 % CO and 98 % CO_2 is expected. This share was chosen for the emission model. In the case of glycine nitrate combustion synthesis, the fraction of CO was estimated as below 1 % for all synthesised metal oxides [41]. However, the CO share is expected to increase with decreasing nitrate content [41]. For combustion of UAN, a share of 4 % CO emissions was measured at 550 °C [39]. At this higher temperature, the Boudouard reaction would suggest a similar share [43]. Hence, the share of 2 % at the applicable calcination temperature of ~450 °C was chosen for this study.

Nitrogen-containing emissions of NO, NO_2, and N_2O were considered. The thermodynamic most stable product of complete combustion would be N_2. However, N_2 peaks are not detectable in MS and FTIR due to the high N_2 concentration in air. The simulation results for combustion of UAN in a flow reactor suggest that the percentage of formed N_2 at 500 °C is below 0.2 % [39]. For glycine nitrate combustion synthesis, the share of N_2 was estimated as ~99 % [41]. However, the reaction during LCNC synthesis does not represent a direct combustion synthesis. MS and FTIR peaks have high intensity for the considered emissions. Therefore, the worst case of 0 % N_2 formation was chosen to prevent underestimation of the EI and unjustified lower impact of the recycling process.

The share of NO, NO_2, and N_2O emissions was estimated based on experimental results by Grinberg Dana et al. for the combustion of UAN [38]. Experimental conditions in LCNC synthesis are most comparable to low flow rates and low pressure. Due to better readability of the data point, the second lowest flow rate of ~1.8 mL min^{-1} and lowest available pressure of 1 MPa were chosen. The measured emissions in mmol of NO (180 mmol per mol ammonium nitrate (AN)), NO_2 (4 mmol per mol AN), and N_2O (150 mmol per mol AN) [38] were used to calculate the shares of 54 %, 1 %, and 45 %, respectively. The dominance of NO and small amount of NO_2 is in line with the general trend at low combustion temperatures [42]. The hydrogen from EDTA, citric acid, and nitric acid was assumed to form H_2O.

The assumed conversion rates for H_2O, NH_3, C, and N enabled calculation of the amount of emitted gases. The required oxygen supply from air was then calculated according to equation (3). All amounts of gases were converted into masses using their molar mass for reporting in the LCI.

Calculated life cycle inventory

The life cycle inventory for the unit process of primary synthesis (1) and recycling (2) of LCNC is listed in Table S10 and S11, respectively. All flows were scaled to a flow of 1 g LCNC powder for better comparability. The list contains all relevant information to model the respective unit process for impact assessment. Due to the focus on new data in the foreground system, the full LCI with all up-stream elemental flows is not presented. Both unit processes fulfil the mass balance due to the approach to model the process emissions. The atomic balance is also maintained.

The quantity of the listed flows is provided with a number of decimal points that is in line with the calculated standard deviation of primary data scaled to 1 g. For the calculation of the model and impact assessment, the calculated average value was used directly.

For comparison of the systems, the different process yields need to be considered. The higher yield of recycling slightly decreases the relative amount of chemicals and electricity per g. A theoretical 5 g metal ion batch should produce 6.01 g of LCNC with the nominal composition. In the case of primary synthesis, 5.62 g (~ 94 %) was produced on average. In the case of recycling, 5.84 g LCNC powder was produced from 6.04 g LCNC input on average. Hence, ~97 % LCNC input was recovered. The slightly higher input (> 6.01 g) during recycling is due to deviations in experimental execution. Amounts of CA and EDTA were also adjusted to the higher input to maintain the stoichiometric ratios.

Specific components of the LCI results are analysed in more detail in the following sections.

Table S10: Input and output flows for primary synthesis of LCNC (1) as a unit process. The standard deviation (SD) was calculated from the available sets of primary data. The quantity is listed with the resulting accuracy. For results of the emission model, three decimal points are given. The calculated mean values were used directly for all calculations and impact assessment.

Input primary synthesis (1)					
Flow	**Type**	**Quantity**	**Unit**	**SD**	**Provider process**
Ammonia solution (25%)	Product	6.7	g	$3 \cdot 10^{-1}$	Production of ammonia solution (25%)
Calcium nitrate	Product	0.1327	g	$6 \cdot 10^{-4}$	market for calcium nitrate | calcium nitrate | Cutoff, S - RER
Citric acid	Product	3.5279	g	$3 \cdot 10^{-4}$	market for citric acid | citric acid | Cutoff, S - GLO
Copper nitrate	Product	0.1633	g	$1 \cdot 10^{-4}$	market for copper nitrate | modified copper sulfate | Cutoff, U - GLO
EDTA, ethylenediaminetetra acetic acid	Product	3.6804	g	$1 \cdot 10^{-4}$	market for EDTA, ethylenediaminetetraacetic acid | EDTA, ethylenediaminetetraacetic acid | Cutoff, S - GLO
Electricity, low voltage, LCNC	Product	1.8	kWh	$4 \cdot 10^{-1}$	market for electricity, low voltage LCNC | electricity, low voltage | Cutoff, S - DE
Lanthanum nitrate	Product	2.1807	g	$2 \cdot 10^{-4}$	market for lanthanum nitrate| modified copper sulfate | Cutoff, U - GLO
Nickel nitrate	Product	0.6094	g	$2 \cdot 10^{-4}$	market for nickel nitrate | modified nickel sulfate | Cutoff, U - GLO
Oxygen	Resource	6.08	g	n/a	n/a
Water, deionised	Product	27	g	4	water production, deionised | water, deionised | Cutoff, S - Europe without Switzerland
Total	Mass	49	g	n/a	

Output primary synthesis (1)					
Flow	**Flow type**	**Quantity**	**Unit**	**SD**	**Specification**
Ammonia	Emission to air	1.675	g	n/a	Germany, high population density
Calcium	Emission to water	0.002	g	n/a	Unspecified
Carbon dioxide	Emission to air	9.774	g	n/a	High population density
Carbon monoxide	Emission to air	0.128	g	n/a	High population density
Copper, ion	Emission to water	0.003	g	n/a	Unspecified
Dinitrogen monoxide	Emission to air	0.465	g	n/a	High population density
Lanthanum - emissions to water	Emission to water	0.045	g	n/a	n/a (no impact assessment)
LCNC Powder	**Product**	**1.00**	**g**	**$1 \cdot 10^{-2}$**	**n/a**
Nickel, ion	Emission to water	0.008	g	n/a	Unspecified
Nitrogen dioxide, DE	Emission to air	0.026	g	n/a	High population density
Nitrogen monoxide	Emission to air	0.760	g	n/a	High population density
Water vapor	Emission	36	g	4	Unspecified
Total	Mass	49	g	n/a	

Table S11: Input and output flows for recycling of LCNC (2) as a unit process. The standard deviation (SD) was calculated from the available sets of primary data. The quantity is listed with the resulting accuracy. For results of the emission model, three decimal points are given. The calculated mean values were used directly for all calculations and impact assessment.

Input recycling (2)					
Flow	**Type**	**Quantity**	**Unit**	**SD**	**Provider process**
Ammonia solution (25%)	Product	8.1	g	$2 \cdot 10^{-1}$	Production of ammonia solution (25%)
Citric acid	Product	3.41	g	$3 \cdot 10^{-2}$	market for citric acid | citric acid | Cutoff, S - GLO
EDTA, ethylenediaminetetraacetic acid	Product	3.56	g	$3 \cdot 10^{-2}$	market for EDTA, ethylenediaminetetraacetic acid | EDTA, ethylenediaminetetraacetic acid | Cutoff, S - GLO
Electricity, low voltage, LCNC	Product	1.8	kWh	$4 \cdot 10^{-1}$	market for electricity, low voltage LCNC | electricity, low voltage | Cutoff, S - DE
LCNC powder	Product	1.035	g	$8 \cdot 10^{-3}$	LCNC secondary material (burden free)
Nitric acid, without water, in 50% solution state	Product	1.870	g	n/a	market for nitric acid, without water, in 50% solution state | nitric acid, without water, in 50% solution state | Cutoff, S - RER w/o RU
Oxygen	Product	5.657	g	n/a	n/a
Water, deionised	Product	56	g	2	water production, deionised | water, deionised | Cutoff, S - Europe without Switzerland
Total	Mass	80	g	n/a	
Output recycling (2)					
Flow	**Flow type**	**Quantity**	**Unit**	**SD**	**Specification**
Ammonia	Emission to air	2.026	g	n/a	Germany, high population density

Calcium	Emission to water	0.001	g	n/a	Unspecified
Carbon dioxide	Emission to air	9.460	g	n/a	High population density
Carbon monoxide	Emission to air	0.124	g	n/a	High population density
Copper, ion	Emission to water	0.001	g	n/a	Unspecified
Dinitrogen monoxide	Emission to air	0.534	g	n/a	High population density
Lanthanum - emissions to water	Emission to water	0.023	g	n/a	n/a (no impact assessment)
LCNC Powder	**Product**	**1.000**	**g**	**$5\cdot10^{-3}$**	**n/a**
Nickel, ion	Emission to water	0.004	g	n/a	Unspecified
Nitrogen dioxide, DE	Emission to air	0.030	g	n/a	High population density
Nitrogen monoxide	Emission to air	0.874	g	n/a	High population density
Water vapor	Emission	65	g	4	Unspecified
Total	Mass	80	g	n/a	

Reactants and process chemicals

The similarity of the Pechini-based processing during the primary synthesis (1) and recycling (2) of LCNC is clearly reflected in the process flows. The main difference between the product systems is the input of primary metal nitrates in system (1). In system (2), burden-free secondary LCNC powder is processed as the source of metal ions.

Very similar amounts of CA and EDTA are utilised in both systems due to the stoichiometric ratio for gelation. However, the higher yield of the recycling process slightly decreases the amount of CA and EDTA per g LCNC by around 3 %.

DI water is used as solvent in both cases. More than twice the amount of water was consumed for recycling because dissolution of LCNC requires more water than the dissolution of metal nitrates. Nitric acid is used as an additional chemical to enable the dissolution of LCNC. This adds additional nitrate ions and protons to the precursor solution. Due to both factors, recycling also requires a larger amount of ammonia solution for adjustment of the pH value. The different consumption of water and ammonia solution are the main reasons for the higher total mass balance in system (2).

Electricity

The electricity consumption per g was slightly higher (+1 %) for recycling than for primary synthesis. The overall electricity consumption per batch was measured as 10.162 kWh and 10.588 kWh for system (1) and (2), respectively. The difference is caused by the additional steps of microwave assisted dissolution and evaporation for recycling. These steps have a contribution of only 4 %. Due to the higher process yield of the recycling process, the difference per g is even lower. The rather high standard deviation of 0.4 kWh is caused by the utilisation of a larger furnace for one calcination data point.

Process emissions

The plausibility of the quantified emissions can be demonstrated by comparison to the measured data. The calculated weight of emissions during the reaction deviate by –3 % and –6 % from the measured weight difference from precursor gel to LCNC powder. In this one-pot approach, every input material that is not incorporated in the LCNC powder leaves the process as emissions.

The same emission types are considered for both product systems. However, their mass varies due to differences in the chemical processes. The larger amount of emitted metal ions in the primary synthesis is due to the unknown stoichiometry of the metal nitrates.

The total mass of gaseous emissions resulting from the model calculations is higher for recycling than for the primary synthesis. The carbon-containing emissions originate from CA and EDTA. Hence, their amount is similar for the two systems. Slightly higher emissions for the primary synthesis originate in the higher relative input of CA and EDTA. All nitrogen-containing emissions are ~ 15 % higher for recycling than for the primary synthesis. The addition of nitric acid adds ~ 41 % more nitrate ions to product system (2) than from metal nitrates in system (1). The emissions do not increase by ~ 41 % due to the comparable input of N from EDTA per batch and the higher process yield of recycling. For ammonia and water emissions, the increased consumption in system (2) is directly reflected in the higher emissions.

The consumed oxygen is calculated from the atomic balance. The 7 % higher oxygen demand in the primary synthesis can be explained by the lower oxygen content of the precursor due to lower nitrate ion content. Hence, more oxygen uptake from air is required to produce LCNC and the considered emissions.

Life cycle impact assessment (LCIA) supplementary information

The cradle-to-gate environmental impact for the primary synthesis (1) and recycling (2) of LCNC powder at laboratory scale are listed in Table 2 (main text) using ILCD 2011 midpoint indicators [44]. Impact indicators with a focus on the effects of process emissions and resource consumption were selected. Note that no normalisation or weighting was applied in this LCA study. Therefore, no cross-comparison between the impact categories or judgement on absolute severity of EI was conducted.

A comparison of the impact values with representative LCA studies for comparable systems can help to evaluate the results. Lee and Hong compared the EI of different proton conducting membranes in a

gate-to-gate approach [35]. A different characterisation model was applied. The same indicator GWP 100 was used for the impact category climate change. The quantified impact per g membrane material in their study ranges from 1.50 kg CO_2 eq to 2.83 kg CO_2 eq, depending on the type of material [35]. The values are in the same order of magnitude as in this study. However, Lee and Hong did not consider process emissions to air from decomposition of the precursor gels [35]. The slightly higher EI in their study could be caused by many experimental factors, such as different equipment and batch size, or true differences from the different raw materials, electricity supply, and synthesis methods. The deviations are thus within the expected order of magnitude. Other available studies did not report the calculated impact values directly.

References

1   R. Baggio and M. Perec, *Inorg. Chem.*, 2004, **43**, 6965–6968.
2   G. Vanhoyland, J. Pagnaer, J. D'Haen, S. Mullens and J. Mullens, *J. Solid State Chem.*, 2005, **178**, 166–171.
3   CRYSTAL IMPACT, *Match! (v. 3.12)*, Bonn, 2021.
4   R. T. Downs and M. Hall-Wallace, *Am. Mineral.*, 2003, **88**, 247–250.
5   S. Gražulis, D. Chateigner, R. T. Downs, A. F. T. Yokochi, M. Quirós, L. Lutterotti, E. Manakova, J. Butkus, P. Moeck and A. Le Bail, *J. Appl. Crystallogr.*, 2009, **42**, 726–729.
6   S. Gražulis, A. Daškevič, A. Merkys, D. Chateigner, L. Lutterotti, M. Quirós, N. R. Serebryanaya, P. Moeck, R. T. Downs and A. Le Bail, *Nucleic Acids Res.*, 2012, **40**, D420-D427.
7   S. Gražulis, A. Merkys, A. Vaitkus and M. Okulič-Kazarinas, *J. Appl. Crystallogr.*, 2015, **48**, 85–91.
8   A. Merkys, A. Vaitkus, J. Butkus, M. Okulič-Kazarinas, V. Kairys and S. Gražulis, *J. Appl. Crystallogr.*, 2016, **49**, 292–301.
9   M. Quirós, S. Gražulis, S. Girdzijauskaitė, A. Merkys and A. Vaitkus, *J. Cheminf.*, 2018, **10**, 23.
10 A. Vaitkus, A. Merkys and S. Gražulis, *J. Appl. Crystallogr.*, 2021, **54**, 661–672.
11 J. Rodriguez-Carvajal, *FullProf. 2k (v. 7.00)*, ILL, Grenoble, 2019.
12 EDAX INC., *Genesis Spectrum (v. 5.21)*, Mahwah, New Jersey, 2007.
13 Netzsch Gerätebau GmbH, *Proteus (v. 6.1)*, Selb, 2015.
14 G. Chen, M. Widenmeyer, B. Tang, L. Kaeswurm, L. Wang, A. Feldhoff and A. Weidenkaff, *Front. Chem. Sci. Eng.*, 2020, **14**, 405–414.
15 H. Wang, C. Tablet, A. Feldhoff and J. Caro, *J. Membr. Sci.*, 2005, **262**, 20–26.
16 D. J. Bogan and C. W. Hand, *The Journal of physical chemistry*, 1971, **75,** 1532-1536.
17 NIST Mass Spectrometry Data Center, William E. Wallace, director, *Acetonitrile mass spectrum,* available at: https://webbook.nist.gov/cgi/cbook.cgi?ID=C75058&Mask=200#Mass-Spec, (accessed 6 April 2022).
18 Coblentz Society, Inc. and NIST Chemistry WebBook, *Nitric oxide,* available at: https://webbook.nist.gov/cgi/cbook.cgi?ID=C10102439&Mask=80, (accessed 6 April 2022).
19 Coblentz Society, Inc. and NIST Chemistry WebBook, *Nitrous oxide,* available at: https://webbook.nist.gov/cgi/cbook.cgi?ID=C10024972&Type=IR-SPEC&Index=1, (accessed 6 April 2022).
20 Coblentz Society, Inc. and NIST Chemistry WebBook, *Ammonia,* available at: https://webbook.nist.gov/cgi/cbook.cgi?ID=C7664417&Type=IR-SPEC&Index=1, (accessed 6 April 2022).
21 Coblentz Society, Inc. and NIST Chemistry WebBook, *Carbon dioxide,* available at: https://webbook.nist.gov/cgi/cbook.cgi?ID=C124389&Type=IR-SPEC&Index=1, (accessed 7 April 2022).

22   Coblentz Society, Inc. and NIST Chemistry WebBook, *Carbon monoxide,* available at: https://webbook.nist.gov/cgi/cbook.cgi?ID=C630080&Type=IR-SPEC&Index=1, (accessed 6 April 2022).

23   Coblentz Society, Inc. and NIST Chemistry WebBook, *Methane,* available at: https://webbook.nist.gov/cgi/cbook.cgi?ID=C74828&Type=IR-SPEC&Index=1, (accessed 6 April 2022).

24   O. Ravkina, J. Räthel and A. Feldhoff, *J. Eur. Ceram. Soc.*, 2015, **35**, 2833–2843.

25   M. Saleem, D. Singh, A. Mishra and D. Varshney, *Mater. Res. Express*, 2019, **6**, 26304.

26   M. Reichmann, P.-M. Geffroy, J. Fouletier, N. Richet and T. Chartier, *J. Power Sources*, 2014, **261**, 175–183.

27   GreenDelta GmbH, *openLCA (v 1.10.3)*, Berlin, 2020.

28   G. Wernet, C. Bauer, B. Steubing, J. Reinhard, E. Moreno-Ruiz and B. Weidema, *The ecoinvent database version 3 (part I): overview and methodology*, Int. J. Life Cycle Assess., 2016, **21**, 1218–1230, available at: http://link.springer.com/10.1007/s11367-016-1087-8, (accessed 28 January 2022).

29   H. P. Corson, Graselli Chemical Company, US Pat., 1,936,829, 1933.

30   J. Zhang and H. W. Richardson, *Copper Compounds; In: Ullmann's Encyclopedia of Industrial Chemistry (Ed.)*, (2016), available at: https://onlinelibrary.wiley.com/doi/10.1002/14356007.a07_567.pub2, (accessed 8 April 2022).

31   A. Nawrocki and R. Olszewki, World Intellectual Property Organization, WO 2006/031139 A1, 2006.

32   L. F. Albright and H. F. Haug, US Pat., 3,348,909, 1967.

33   G. Horn, J. Lohr, K. Moraw and W. Materne, US Pat., 5,039,502, 1991.

34   B. Agarski, V. Nikolić, Ž. Kamberović, Z. Anđić, B. Kosec and I. Budak, *J. Cleaner Prod.*, 2017, **162**, 7–15.

35   S.-S. Lee and T.-W. Hong, *Materials*, 2014, **7**, 6677–6685.

36   L. Zhao and J. Brouwer, *ECS Trans.*, 2012, **42**, 247–263.

37   Y. Li, B. Tan and Y. Wu, *Chem. Mater.*, 2008, **20**, 567–576.

38   A. Grinberg Dana, G. E. Shter and G. S. Grader, *RSC Adv.*, 2014, **4**, 10051–10059.

39   A. Grinberg Dana, B. Mosevitzky, G. Tvil, M. Epstein, G. E. Shter and G. S. Grader, *Energy Fuels*, 2016, **30**, 2474–2477.

40   A. Grinberg Dana, O. Elishav, A. Bardow, G. E. Shter and G. S. Grader, *Angew. Chem., Int. Ed. Engl.*, 2016, **55**, 8798–8805.

41   T. Pine, X. Lu, D. R. Mumm, G. S. Samuelsen and J. Brouwer, *J. Am. Ceram. Soc.*, 2007, **90**, 3735-3740.

42   S. R. Turns, *Introduction to Combustion. Concepts and Applications*, McGraw-Hill Companies New York, New York, 2nd edn., 2006.

43   A. F. Holleman and E. Wiberg, *Lehrbuch der Anorganischen Chemie (91.-100. Auflage)*, Walter de Gruyter GmbH & Co., Berlin, 91st edn., 1985.

44   European Commission, Joint Research Centre, Institute for Environment and Sustainability, *Characterisation factors of the ILCD Recommended Life Cycle Impact Assessment methods. Database and supporting information*, Publications Office of the European Union, Ispra, 2012.